AD-754 087

EFFECTS OF STRONG EXPLOSIONS. V. (SOVIET LITERATURE TRANSLATIONS)

Simon Kassel

RAND Corporation

Prepared for:

Advanced Research Projects Agency

August 1972

ARPA ORDER NO.: 189-1

R-760/4-ARPA
August 1972

EFFECTS OF STRONG EXPLOSIONS – V
(Soviet Literature Translations)

Compiled by Simon Kassel

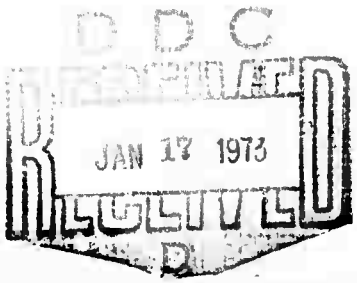

A Report prepared for

ADVANCED RESEARCH PROJECTS AGENCY

Rand
SANTA MONICA, CA. 90406

This research is supported by the Advanced Research Projects Agency under Contract No. DAHC15 67 C 0141. Views or conclusions contained in this study should not be interpreted as representing the official opinion or policy of Rand or of ARPA.

DOCUMENT CONTROL DATA

1. ORIGINATING ACTIVITY The Rand Corporation	2a. REPORT SECURITY CLASSIFICATION UNCLASSIFIED 2b. GROUP

3. REPORT TITLE

EFFECTS OF STRONG EXPLOSIONS - V (Soviet Literature Translations)

4. AUTHOR(S) (Last name, first name, initial)

Compiled by Kassel, S.

5. REPORT DATE	6a. TOTAL NO. OF PAGES	6b. NO. OF REFS.
August 1972	~~65~~ 66	

7. CONTRACT OR GRANT NO.	8. ORIGINATOR'S REPORT NO.
DAHC15 67 C 0141	R-760/4-ARPA

9a. AVAILABILITY/LIMITATION NOTICES	9b. SPONSORING AGENCY
DDC-A	Defense Advanced Research Projects Agency

10. ABSTRACT

English-language abstracts prepared by Informatics, Inc., of about 45 Soviet technical writings on the effects of strong explosions, particular nuclear explosions, and their simulation under laboratory and field conditions. The articles abstracted appeared in 1971 and early 1972. The abstracts are arranged under these general headings: (1) shock waves in gas; (2) equations of state for gas; (3) exploding wires; (4) hypersonic flow past bodies; (5) atmospheric physics; (6) soil mechanics; (7) laser simulation and related effects; (8) particle beams; and (9) electromagnetic field interaction with materials. The abstracts vary in length according to the pertinence and significance of the original papers. The usual glossary of journal abbreviations is included.

11. KEY WORDS

USSR--Science
Nuclear Explosions
Atmosphere
Physics
Fluid Dynamics
Gas Dynamics
Lasers

I-a

ARPA ORDER NO.: 189-1

R-760/4-ARPA
August 1972

EFFECTS OF STRONG EXPLOSIONS – V
(Soviet Literature Translations)

Compiled by Simon Kassel

A Report prepared for

ADVANCED RESEARCH PROJECTS AGENCY

Rand
SANTA MONICA, CA. 90406

Bibliographies of Selected Rand Publications

Rand maintains a number of special subject bibliographies containing abstracts of Rand publications in fields of wide current interest. The following bibliographies are available upon request:

Aerodynamics • Arms Control • China • Civil Defense
Communication Satellites • Communication Systems
Computer Simulation • Computing Technology
Decisionmaking • Game Theory • Maintenance • Middle East
Policy Sciences • Probability • Program Budgeting
SIMSCRIPT and Its Applications • Southeast Asia
Space Technology and Planning • Statistics • Systems Analysis
USSR/East Europe • Weapon Systems Acquisition
Weather Forecasting and Control

To obtain copies of these bibliographies, and to receive information on how to obtain copies of individual publications, write to: Publications Department, Rand, 1700 Main Street, Santa Monica, California 90406.

Published by The Rand Corporation

II

PREFACE

This Report is one in a series entitled "Effects of Strong Explosions" and intended to provide an overview of current Soviet research activities in that field. It falls within the scope of a continuing program, sponsored by the Defense Advanced Research Projects Agency, which undertakes the systematic coverage of selected areas of Soviet scientific and technological literature.

The effects of strong explosions, particularly nuclear explosions, and their simulation under laboratory and field conditions involve a very broad range of phenomena and parameters such as high temperatures, pressures, electromagnetic energy densities, interaction of energy with materials, shock waves in gases, liquid, and solids, and, in general, events occurring under conditions of a high degree of mechanical, thermal, and radiation stress. The series of Rand Reports of which this is the fifth to be published will cover a variety of the pertinent topics as they are reflected in the currently available Soviet literature, by supplying abstracts from and summaries of the scientific and technological publications of the USSR.

The material in the present Report is derived exclusively from Soviet technical writings that appeared in 1971 and the early part of 1972. The abstracts here included were prepared by Informatics, Inc. They have been arranged by the compiler according to fairly general subject areas, and vary in length depending on the pertinence and significance of the individual papers.

The information assembled in this Report covers our most recent knowledge of Soviet research on the effects of explosions, and should prove useful to American scientists working in this and related fields of research.

CONTENTS

KEY TO JOURNAL ABBREVIATIONS

DAN BSSR	Doklady akademii nauk Belorusskoy SSR (Reports of the Academy of Sciences of the Belorussian SSR)
FAiO	Akademiya nauk SSR. Izvestiya. Fizika atmosfery i okeana (Academy of Sciences, USSR, News, Atmospheric and oceanic physics)
FGiV	Fizika goreniya i vzryva (Physics of combustion and explosion)
FTT	Fizika tverdogo tela (Solid-state physics)
I-FZh	Inzhenerno-fizicheskiy zhurnal (Engineering physics journal)
IVUZ Radiofiz	Izvestiya vysshikh uchebnykh zavedeniy. Radiofizika (Radiophysics)
FiKhOM	Fizika i khimiya obrabotki materialov (Physics and chemistry of materials processing)
MZhiG	Mekhanika zhidkosti i gaza (Mechanics of liquid and gas)
OMP	Optiko-mekhanicheskaya promyshlennost' (Optical and mechanical industry)
PTE	Pribory i tekhnika eksperimenta (Instruments and technology for experiments)
UFZh	Ukrainskiy fizicheskiy zhurnal (Ukrainian journal of physics)
VAN Kaz SSR	Akademiya nauk Kazakhskoy SSR. Vestnik (Academy of Sciences, Kazakh SSR, Herald)
ZhETF	Zhurnal eksperimental'noy i teoreticheskoy fiziki (Journal of experimental and theoretical physics)
ZhETF P	Zhurnal eksperimental'noy i teoreticheskoy fiziki, Pis'ma (Journal of experimental and theoretical physics, Letters)

ZhPMTF	Zhurnal prikladnoy mekhaniki i tekhnicheskoy fiziki (Journal of applied mechanics and technical physics)
ZhPS	Zhurnal prikladnoy spektroskopii (Journal of applied spectroscopy)
ZhTF	Zhurnal tekhnicheskoy fiziki (Journal of technical physics)

I. SHOCK WAVES IN GAS

Aleksandrov, V. V. Phase plane method for solution of one-dimensional problems in radiative gas dynamics. MZhiG, no. 1, 1972, 144-155.

The phase plane method is used to solve the problem of one-dimensional equilibrium flow of an inviscid, radiating, absorbing, and scattering gas. For gas propagation with strong radiation interference, the usual numerical solution to this problem, based on Peierls equation of radiant emission Was a function of optical depth τ, becomes complicated because of boundary layer formation behind a shock wave. For that reason the problem is formulated in different material coordinates; namely, dimensionless gas velocity V and W, in the (V, W) or "phase plane". In the presence of scattering and strong radiation interference with gas propagation, such an approach is preferable to using the Peierls equation, because the V of one-dimensional gas flow is a measure of both kinetic and internal gas energies. The phase plane thus represents an energetic space with the energy characteristics of the substance and radiation as coordinates. The function W(V) for gray body radiation is determined by the nonlinear integral equation

$$w(v) = \frac{B}{2}\int_{v_0}^{1} \{[1-\lambda(\xi)]\theta^4(\xi) + \lambda(\xi)w(\xi)\}K[\xi, w(\xi)]\times \\ \times E_1\left\{B\left|\int_{\xi}^{\infty} K[\eta, w(\eta)]d\eta\right|\right\} d\xi \qquad (1)$$

where B = Bo/4 is the Boltzmann constant, Θ is the dimensionless gas temperature, K is the absorption coefficient, ξ, E_1, and η are values from Peierls equation in neutron transport theory. Solution of (1) gives W(V). The phase plane (V, W) for selective radiation has an infinite dimension, and the problem for a nonscattering gas is therefore formulated by the equation of energy

$$q(v) = -\frac{\pi^3 k_P(v)}{15}\theta^4(v) + \frac{\pi B_s}{2}\int_{v_0}^{1} \frac{d\xi}{q(\xi)}\left(\frac{dh}{d\xi}+\xi\right)\times \\ \times \int_0^{\infty} dy k(v,y)k(\xi,y)P(\xi,y)E_1\left\{B_s\left|\int_{\xi}^{\infty}\frac{k(\eta,y)}{q(\eta)}\left(\frac{dh}{d\eta}+\eta\right)d\eta\right|\right\} \qquad (2)$$

where q is the volumetric rate of gas energy increase due to radiation, $B_s = \frac{\pi^5}{60}$ Bo, Kp, K, h, y, and P are the dimensionless Planck absorption

coefficient, optical constant, enthalpy, frequency, and Planck function, respectively.

Application of formulas (1) and (2) is illustrated by examples of a strong shock wave propagating in a cold, transparent, nonscattering gas and a shock wave propagating in a radiating, absorbing, and scattering gas with strong radiation interference. In the first example, a formula derived from (1) for the Θ of a gray body shows that the gas is strongly cooled by radiation. The discontinuity of shock wave velocity is formulated in the second example for a perfect gas in a diffusion approximation of the radiation transport equation in the phase plane. It is shown that discontinuity exists at $\gamma < 2$ and $M_1 > 1.5$ or > 2.05 in the incident flow.

Simonov, I. V. Diffraction of a strong shock wave on a weakly-defined wedge. ZhPMTF, no. 6, 1971, 107-114.

A theoretical study is presented on diffraction of a strong two-dimensional steady shock wave on a wedge whose properties (initial density, behavior under impact load) differ only slightly from those of the medium in which the shock wave propagates. A linear approximation of diffraction - initiated small perturbations, disregarding differences in strength and sound velocity c in the medium and wedge, is justified under conditions of high pressure ($\sim 10^6$ atm) and temperature behind the strong shock wavefront. The validity of the approximation is supported by the fact that the effect of strength characteristics diminishes with increased shock wave intensity. In this approximation, the unknown perturbation velocity components u' and w' and perturbation pressure p' satisfy the ordinary linear equations for the two-dimensional flow of an ideal compressible fluid. The equations are given in the form

$$Dp = \frac{\partial u}{\partial x} + \frac{\partial w}{\partial y}, \quad Du = \frac{\partial p}{\partial x}, \quad Dw = \frac{\partial p}{\partial y} \quad \left(D = x\frac{\partial}{\partial x} + y\frac{\partial}{\partial y}\right) \tag{1}$$

where u, w, and p are dimensionless variables. Conditions in the perturbation region of the shock wavefront are described by

$$p = A(f - yf'), \quad u = Bp, \quad w = -Mf' \text{ at } x = k \tag{2}$$

in the medium, and

$$p = A(f - yf') + A_1, \quad u = Bp + B_1, \quad w = -Mf' \text{ at } x = k$$
$$A = \frac{2\varkappa M}{1-j}, \quad A_1 = kM\frac{(2\varkappa - 1)v' - \varkappa v_0}{(1-j)(1-\varkappa)}, \quad B = \frac{1+j}{2k} \tag{3}$$
$$B_1 = M\frac{v' - \varkappa v_0}{2(1-\varkappa)} \quad \left(\varkappa = \frac{V_0}{V}, \quad M = \frac{U_0}{c}, \quad k = \frac{D_0 - U_0}{c}, \quad j = \frac{k^2c^2 j_0}{V_0}\right)$$

in the wedge. Vo and Uo in (3) are specific volume and mass velocity, respectively, behind the shock wavefront, and V is the specific volume of the medium ahead of the front. The problem was reduced to determining the function p(x, y), which is continuous along the discontinuity boundary line. Two possible diffraction wave configurations are examined. At wedge angles $\alpha_1, \alpha_2 < \alpha_*$, the limit angle, a triple configuration (Fig. 1) forms near the

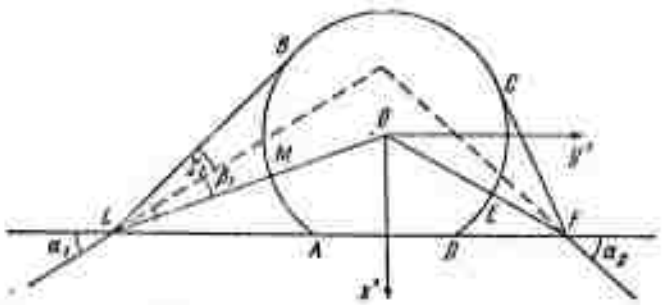

Fig. 1. Diffraction pattern at $\alpha_1, \alpha_2 < \alpha_*$.

intersections L and F of the shock wave with the edges of a wedge. The nonstationary perturbation from the shifted wedge center O propagates within the region bounded by the ABCD arc of the Mach circle, the attached reflected acoustic wavefronts, and the AD portion of the shock wave. At $\alpha_{1,2} > \alpha_*$, there is an irregular refraction near L and F and only one region of nonstationary flow, which includes the shock wave sections outside the wedge (Fig. 2).

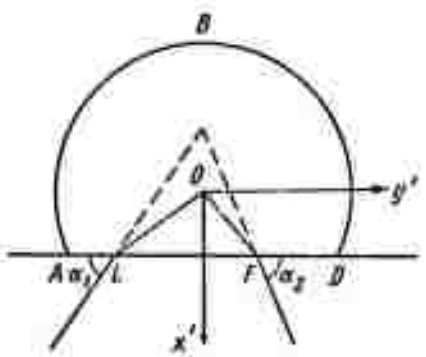

Fig. 2. Diffraction pattern at $\alpha_1, \alpha_2 > \alpha_*$.

The α_* value in the system of x'y' coordinates is determined by

$$\alpha_* = \arcsin\left(k_0 / \sqrt{k_1^2 + k_0^2}\right) \qquad (k_1 = \sqrt{1 - k^2}) \tag{4}$$

where $k_o = D_o/C_o$, D_o = shock wave velocity.

In any case, the problem of determining p(x, y) is transferred into the plane $Z = x_1 + iy_1$ (Fig. 3) and the lune is represented conformally

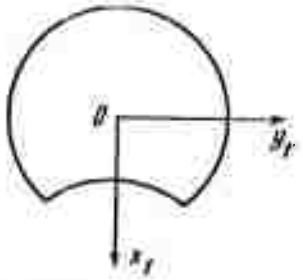

Fig. 3. Region of nonstationary flow in the Z complex plane.

on the upper half-plane ζ by means of the transform

$$\zeta = \xi + i\eta = \frac{i}{k_1}\frac{2z - k(1 + z^2)}{z^2 - 1} \tag{5}$$

The analytical function $F^+(\zeta)$ of ζ half-plane satisfies the condition

$$a\frac{\partial p}{\partial \eta} + b\frac{\partial p}{\partial \xi} = d \tag{6}$$

where

$$\begin{gathered}
a = \xi\sqrt{1-\xi^2}, \quad b = B\xi^2 - B_2 \qquad (|\xi| < 1) \\
a = 0, \quad b = B - B_2 \qquad (|\xi| > 1) \\
d = (B - B_2)(p_1\delta(\xi - \xi_1) - p_2\delta(\xi - \xi_2)) \qquad (\alpha_{1,2} < \alpha_*) \\
d = (B_1\xi^2 + A_1B_2)(\delta(\xi - \xi_3) - \delta(\xi - \xi_4)) \qquad (\alpha_{1,2} > \alpha_*) \\
\xi_1 = \xi_B = k_1^{-1}(\operatorname{cosec}\theta_1 - k\operatorname{ctg}\theta_1), \quad \xi_2 = \xi_C = k_1^{-1}(\operatorname{cosec}\theta_2 - k\operatorname{ctg}\theta_2) \\
\xi_3 = \xi_L = -\varkappa^{-1}\operatorname{ctg}\alpha_1, \quad \xi_4 = \xi_P = \varkappa^{-1}\operatorname{ctg}\alpha_2
\end{gathered} \tag{7}$$

and $\delta(\Theta)$ is a Dirac function.

The formulas (6) and (7) represent the inhomogeneous Hilbert problem with continuous parameters. The problem is solved by determining the function having a zero point not lower than second order at infinity. The solution must satisfy the condition

$$0 < k^2(1 - j) < \varkappa k_1^2(1 + j) \tag{8}$$

which is equivalent to the condition of stability of a two-dimensional stationary shock wave in a homogeneous medium. The boundary $\Phi^+(\xi)$ of the analytical function

$$\Phi^+(\zeta) = \frac{1}{B\zeta^2 - B_2 + i\zeta\sqrt{1-\zeta^2}} \tag{9}$$

satisfies the condition (8), since it does not exhibit singularities in the upper half-plane. The function $F^+(\zeta)/\Phi^+(\zeta)$ must be regular at infinity. It follows that

$$F^+(\zeta) = \Phi^+(\zeta)[\Psi^+(\zeta) + C_0] \tag{10}$$

where

$$\psi^+(\zeta) = \begin{cases} \frac{1}{\pi}\left(\frac{p_1}{\Phi^+(\xi_1)(\xi_1-\zeta)} - \frac{p_2}{\Phi^+(\xi_2)(\xi_2-\zeta)}\right), & \alpha_{1,2} < \alpha_* \\ \frac{1}{\pi}\left(\frac{B_1\xi_4^2 + A_1B_2}{\xi_4-\zeta} - \frac{B_1\xi_3^2 + A_1B_2}{\xi_3-\zeta}\right), & \alpha_{1,2} > \alpha_* \end{cases} \tag{11}$$

The constant C_0 in (10) is determined from the condition of smooth conjugation of the wavefront.

Pressure is determined from

$$p(\xi, \eta) = \operatorname{Im} \int_{-1}^{\xi} \left(\frac{\partial p}{\partial \eta} + i\frac{\partial p}{\partial \xi}\right) d\zeta + p_A \tag{12}$$

where $p_A = p_1$ for $\alpha_{1,2} < \alpha_*$ and $p_A = 0$ for $\alpha_{1,2} > \alpha_*$.

Pressure, as well as f', u, and w, exhibit a logarithmic singularity in L and F. A formula is also derived for p distribution p(y) along the curved section AD of the shock wave. The functions u and w are determined from (1) and expressed in terms of p in a closed system of equations.

It is noted that the results obtained may contribute to the development of a theory of irregular refraction.

Salamandra, G. D. and N. M. Ventsel'. Measurement of gas velocity with the use of the contact discontinuity surface. ZhTF, no. 11, 1971, 2463-2465.

A method is described for gas velocity measurements behind a detonation wave front. The contact discontinuity surface formed in the gas is used as the point of reference for gas motion; the contact discontinuity surface is assumed to be formed by the interaction between shock and detonation waves. The surface is visualized by the Toepler technique. For several experiments, the numerical value of gas velocity measured 16% lower

than the theoretical value. Shock tube experiments show that the contact discontinuity surface can give a reasonably accurate value of shock wave velocity, and can furthermore serve as a reference for evaluating other velocity measurement references, e.g. the heat inhomogeneity technique.

Zaydel', R. M. Shock wave passage through a curved boundary interface between two media. MZhiG, no. 1, 1972, 111-121.

Shock wave interaction with a slightly curved boundary surface and shock wave-induced surface motion are analyzed in an x-y coordinate system. The shock wave theoretically propagates with velocity D_o through a light medium ($X > 0$) toward the boundary surface $X = 0$ and interacts with it during the time $\tau = 2\ a_o/D_o$ (Fig. 1). During the interval τ, the A point

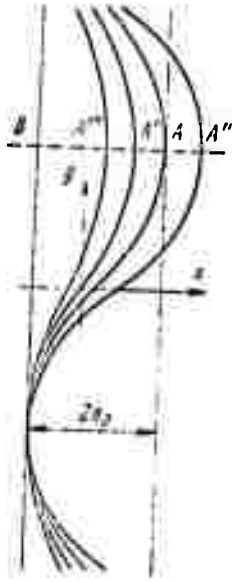

Fig. 1. Shock wave interaction with the free-stream interface $X = 0$ between two media.

shifts to A' and the points between A and A' are distributed at a time τ along the boundary

$$a = a_0 \exp(ikY) \qquad (1)$$

where $ka_0 \leq 1$ is a small perturbation. The free-stream boundary is set in motion after τ at a velocity U relative to an uncompressed heavy medium ($X < 0$). V_1 and V_2 are the relative velocities of the reflected and transmitted shock waves. A set of gas dynamic equations with boundary and initial

conditions is formulated for small perturbations. Introducing polar hyperbolic variables

$$y_s = r_s \operatorname{ch}\theta_s, \quad x_s = r_s \operatorname{sh}\theta_s, \quad r_s = \sqrt{y_s^2 - x_s^2}, \quad \operatorname{th}\theta_s = x_s / y_s \tag{2}$$

and using a Laplace transform, the author obtains a solution to the equations in the general form

$$w_s''(q_s, \theta_s) = F_s(q_s + \theta_s) + \Phi_s(q_s - \theta_s) \quad (s = 1, 2) \tag{3}$$

where F and Φ are arbitrary functions, $p_s = \sinh g_s$, s = 1 in the $0 < X < V_1 t$ region, and s = 2 in the $-V_2 t < X < 0$ region. Integration of the original gas dynamic equation in polar hyperbolic coordinates, using (3), gives three finite difference equations which have a unique solution in the form of expansion in an exponential series. In the $\Delta p \longrightarrow 0$ approximation, where Δp is the shock wave intensity, the solution is

$$\Phi_1(q_1) = -\tfrac{1}{2} v_1^{\circ} e^{-q_1}, \qquad F_2(q_2) = \tfrac{1}{2} v_2^{\circ} e^{-q_2} \tag{4}$$

$$u(t) = k a_0 U \psi(\tau) \qquad (\tau = k c_1 t)$$

$$\psi(\tau) = \frac{1}{2\pi i} \int \Psi(p) e^{p\tau}\, dp = \int_0^{\tau} \psi_1(x)\, dx + \psi_2(\tau) + \psi_3(\tau) \tag{5}$$

where

$$\Psi(p) = p^{-1}\Psi_1(p) + \Psi_2(p) + \Psi_3(p)$$

$$\Psi_1(p) = (1-\mu)\,[\mu/r + 1/R]^{-1}, \quad \Psi_2(p) = (\mu - 1/\alpha)\,[\mu + r/R]^{-1},$$

$$\Psi_3(p) = (1-\alpha)\,[1 + \mu R/r]^{-1}, \quad r = \sqrt{p^2+1}, \quad R = \sqrt{\alpha^2 p^2 + 1} \tag{6}$$

is the transform of $\Psi_1(p)$. c_1 is the sound velocity in the s = 1 region, $\mu = \rho_1/\rho_2$, and $\alpha = c_1/c_2$. Expression (6) is simplified in the cases of $\alpha = 1$ ($c_1 = c_2$), $\rho_1 = \rho_2$ ($\mu = 1$), or the acoustic impedance $\rho_1 c_1 = \rho_2 c_2$ ($\lambda = \alpha\mu = 1$). Integration of (5) gives the asymptotic value

$$\psi(\tau \to \infty) = \text{const} = \frac{1-\mu}{1+\mu} = \frac{\rho_2 - \rho_1}{\rho_2 + \rho_1} \tag{7}$$

i.e. $\Psi(\tau)$ depends on the ρ_1/ρ_2 ratio only. A generalization of the conclusion led to an equation of motion for the free-stream boundary

$$\frac{d^2 a}{dt^2} = \frac{\rho_2 - \rho_1}{\rho_2 + \rho_1} k g a \tag{8}$$

where the acceleration g = NU, and N is the number of incident shock waves, each imparting ΔU acceleration to the boundary interface. This equation is identical to the equation of Rayleigh-Taylor for gravitational instability of noncompressible fluids. It is concluded that the effect of compressibility is insignificant when the wavelength of boundary perturbations is sufficiently small.

Shifrin, E. G. Study of a "hanging" shock wave near the point of origin. MZhiG, no. 6, 1971, 30-37.

Mapping of a "hanging" compression shock into a hodograph plane is described for a two-dimensional, nonuniform supersonic flow in a perfect gas. A general analytical solution of the shock at its point of origin is obtained in the hodograph plane by the method of asymptotic expansions in first and second order approximations. Shock formation conditions are formulated at a supersonic point of flow. It is shown that a quadratic parabolic form of the boundary line in the hodograph plane is a necessary condition of shock formation at a supersonic point in a physical plane in which convolution is present.

Khristoforov, B. D. Small-scale electromagnet for explosion investigations. PTE, no. 1, 1972, 251.

An electromagnet has been built for laboratory measurements of the mass and wave velocities of shock and detonation waves. The field of intensity across a 200 x 200 x 200 mm^3 gap is ~400 Oe; in addition there is a permanent magnetic field which extends over a 50 x 50 x 40 mm^3 region near the gap center. The 70 mm diameter magnetic circuit is made of 900 x 900 mm^2 Armco iron. The corners of the device are strengthened by welding and special straps to increase resistance to explosive loads. Dimensions of the magnet gap and the permanent magnetic field are controlled by specially designed pole shoes made of a 200 mm dia type St. 3 steel. The field intensity across the gap can be increased in inverse ratio to the end-area of a tapered attachment to the pole shoe. Two paralleled magnetic coils, each composed of 2000 turns of 1.8 mm copper wire, are used for superposed magnetization. The 24 volt current supply is supplied by a VSA6 rectifier. The magnetic circuit is installed in a channel welded from channel bars; the channel itself is welded to a table made of angle steel to increase the rigidity of the assembly. Over the past three years, the electromagnet has withstood several hundred detonations of explosive charges up to 0.5 kg without substantial damage. A photograph of the electromagnet assembly is included.

Nevskiy, L. B. Application of interferometer mirror shift for gas dynamic investigations. OMP, no. 2, 1972, 9-11.

A quantitative analysis is presented of the shift of supersonic gas flow interferograms, which were obtained with a dual beam shift interferometer with a spherical mirror in a reflected divergent optical beam. In contrast to a polarization shift interferometer, this interferometer allows

a smooth and uncomplicated shift of the wavefront. Integral equations were derived for flow densities $\rho_\nu^* = \rho_\lambda / \rho_\infty$, where ρ_∞ is the density of incident flow; and ρ_s^*, where the ν and s subscripts indicate, the points of an interferogram along the section under study and the points between which ρ^* is to be determined. The equations for ρ_ν^* and ρ_s^* can be used for small and large shifts of wavefront, respectively, if the shift interferometer is used as a shadow instrument attachment for the study of axisymmetrical inhomogeneities. It is assumed that shift interferograms with large and small shifts in wavefronts are obtained simultaneously and successively for a steady flow.

Experimental data obtained from the shift interferograms are compared with theoretical aerodynamic data and experimental data obtained from Mach-Zender interferograms. Theoretical and interferometric $\rho^*(\xi)$ plots (where ξ is a coordinate) for a $M_\infty = 2$ flow around a sharp-nosed cone with a 15° apex half-angle exhibit an ~8% discrepancy at the edge of inhomogeneity. For a $M_\infty = 2$ flow around a hemisphere cylinder, the $\rho^*(\xi)$ plots obtained for three sections from the shift interferograms, using either the ρ_ν^* or ρ_s^* formula, deviated by 8-10% from plots obtained with the Mach-Zender interferometer for the same sections.

Gorelov, V. A., and L. A. Kil'dyushova. An experimental study of parameters of ionized air in front of a strong shock wave. MZhiG, no. 6, 1971, 17-22.

Electron density n_e and elctron diffusion velocity in ionized air ahead of a strong shock wave (V_s = 10-12.5 km/sec) were measured in an electric discharge shock tube at an initial pressure p_0 = 0.2 torr. A resonance shf probe was used for the n_e measurements to verify earlier data obtained by the authors with a standard probe (MZhiG, no. 2, 1971, 147). A conductor wire shortcircuited at both ends was used as a resonance system. The wire was placed along the shock tube diameter and connected to the feed system and a measuring line; the feed system was connected to the shf-generator (f = 5.8-6.7 GHz). Resonance of the shorted wire appeared at the instant when effective length l was $1/2\ N\lambda$, where N is the number of half-waves on the wire. The instant was recorded as a characteristic spike on an oscilloscope trace. The corresponding n_e was calculated to be 2.8×10^{11} cm^{-3} as compared to the 2.2×10^{11} cm^{-3} value measured with a double probe (at V_s = 11.2 km/sec). The n_e values obtained by the two methods differ by ~ 30%, as shown on an $n_e = f(x)$ plot, where x is the distance to the shock wavefront. Ba atoms were injected into the tube near the measuring probe but did not affect the n_e level.

The electron mass velocity U_e // in the direction of shock wave propagation was measured to determine the effect of free-electron diffusion into the region of precursor ionization. An electromagnetic induction method was used, based on measurement of the potential difference at the boundary of the plasma flow through a transverse magnetic field. The experimental U_e versus x plots show that the measured U_e // values near the shock front are in satisfactory agreement with those calculated for a free diffusion, but they decrease rapidly with increases in distance from the front approaching values corresponding to ambipolar diffusion.

Ivanov, A. A., L. L. Kozorovitskiy, V. D. Rusanov, R. Z. Sagdeyev, and D. P. Sobolenko. Experimental observation of electron shock waves in a collisionless plasma. ZhETF P, v. 14, 1971, 593-596.

Experiments are described which establish the existence of a stationary thermal discontinuity, or electron shock wave, in a collisionless plasma. Tests were done in hydrogen, argon, and xenon, using a plasma generated in a glass tube by two shf generators and an axial magnetic field in the 0.5--5 koe range. Local heating of the plasma to electron temperatures of some 300 ev was induced by a single-turn high current coil generating a large magnetoacoustic wave whose energy was absorbed by the plasma in the coil region. Probe data of nT vs. axial position then show a drop in nT and pressure characteristic of a shock wave. Variation in wavefront parameters were investigated under different test conditions; these showed that the length and velocity of the wavefront were independent of initial electron temperature. Tolerably good agreement was found between theory and experiment for the argon and hydrogen shock data. The tests thus confirm the possibility of a stationary electron shock wave in a collisionless plasma; analogous results could occur from effective braking of a relativistic high-current beam in plasma.

II. EQUATIONS OF STATE FOR GAS

Stesik, L. N. Calculation of detonation parameters of explosive mixtures with metals using an equation of state for perfect gases. FGiV, no. 1, 1971, 111-117.

Detonation parameters and composition of detonation products are computed, using formulas derived for a system satisfying an equation of state for perfect gases. Detonation velocity D is determined mainly by the relationship of two opposing factors: the heat Q released in a detonation wave and the fraction of a condensed phase in the products. Tabulated theoretical data and plots of D and Q versus metal percentages led to the conclusion that the D of the metal mixtures (Al, Be, B) in explosives having a negative oxygen balance (TEN, pyroxylin, RDX, TNT) increases by only 2-5% with an increase in metal content, while D in mixtures of Al with oxydants (hexanitroethane, ammonium nitrate or perchlorate) may increase by 10-30%.

III. EXPLODING WIRES

Yel'yashevich, M. .., A. A. Labuda, L. Ya. Min'ko, I. G. Nekrashevich, G. M. Novik, and G. I. Bakanovich. Pulsed accelerator generation of high-velocity plasma beams based on electric explosion of wires and dielectric erosion. DAN BSSR, v. 16, no. 2, 1972, 115-117.

An improved pulsed generator of moving plasma is described. Plasma is produced by an electric explosion of wires in a discharge chamber of specific geometry and dimensions. In one version, metallic plasma is produced by electric explosion. Breakdown of current flow is eliminated by using an exploding conductor in the form of a thin metallic film deposited on the inner surface of a dielectric insert in the discharge chamber. Loss of stored capacitor energy is avoided by placing the discharge gap inside the chamber (Fig. 1). In a second version, a pulsed surface discharge, without

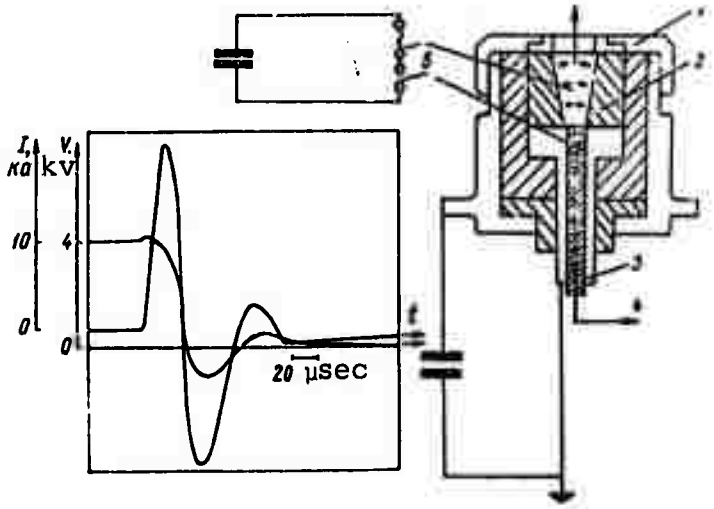

Fig. 1. Pulsed generator and typical oscilloscope trace of a discharge:
1- ring electrode
2- dielectric insert
3- central electrode
4- firing electrode
5- diagram of the auxiliary and internal gaps of the plasma generator using electric explosion of wires

metallic film, is used to promote erosion plasma. At V = 4kv and C = 200mf in the first version, 1.3 kj was discharged for a 1.6 kj initial energy. The calculated energy characteristics of the plasma generation under the cited

conditions are plotted. The erosion plasma beams produced at V = 5kv and C = 1950 mf were recorded by high-speed photography.

In both versions described, underexpanded hypersonic plasma beams can be produced at atmospheric pressure. A low-temperature metallic plasma beam of a predetermined composition is produced with a relatively high efficiency in the first version of the generator. The optimum exit velocity of plasma was 25 km/sec. A relatively dense ($n_e = 5 \times 10^{16}$ cm^{-3}) low-temperature (6000° K) erosion plasma is formed in the second generator. The erosion plasma exhibits characteristic high-intensity continuous and line spectra.

IV. HYPERSONIC FLOW PAST BODIES

Filatov, Ye. I. The optimum shape of a lifting body at hypersonic speeds. MZhiG, no. 1, 1972, 82-86.

Optimization of the aerodynamic characteristics of a horizontally flying hypersonic body is attempted, omitting some previous simplifying assumptions. The body is given a rectilinear coordinate system in which directions of the x and z axes are opposite to the flight direction and vertically downward, respectively. It is assumed that xz is the symmetry plane; that $z = my$ and $z = f(x, y)$ are the upper and lower boundary planes of the semi-body $y \geq 0$, and that the rectilinear leading edge is formed by intersection of the $z = my$ and $x = ky$ planes. It is further assumed that the bottom section is in the $x = k\ell = \ell_1$ plane, where ℓ is the semi-span; the function $f(x, y)$ can be approximated by a polynomial of a low order in any $x = \text{const}$, $y = \text{const}$ section, and that the thickness of the leading edge is negligibly small in relation to the characteristic dimension of the optimum body in the z direction, i.e. at $x = ky$ and $f(x, y) = mz$. The optimum body shape problem is then formulated in terms of a variational method. Solution of the problem is reduced to finding, within the class $\zeta = \zeta(\xi, \eta)$ of surfaces satisfying the condition $\zeta(0, \eta) = 0$, a surface which would satisfy the maximum value of the functional

$$K = (Y_1 + Y_2)\,(X_1 + X_2)^{-1} \tag{1}$$

where X_1, X_2 are the drag factors relative to the double velocity head on the semi-body and its leading edge, respectively, and Y_1, Y_2 are the corresponding relative lift forces. The volume of the semi-body must be $V = \text{const}$, and the m, ℓ, and k parameters are assumed to vary with surface geometry. The new coordinates

$$\xi = (x - ky)/l, \quad \eta = y/l, \quad \zeta = (z - my)/l$$
$$p = \frac{\partial \zeta}{\partial \xi}, \quad q = \frac{\partial \zeta}{\partial \eta} - pk + m \tag{2}$$

are introduced in the solution. Using the Ritz method, the unknown optimum surface is described by the equation

$$\begin{aligned}\zeta = \xi\{&6/k^2l^3 + a_{11}(\eta - 0.25) + \\ &+ a_{12}(\eta - 0.1) + \\ &+ a_{20}(\xi - k/2) + a_{21}(\xi\eta - \\ &- k/10) + a_{22}(\xi\eta^2 - \\ &- k/30) + \ldots\}\end{aligned} \tag{3}$$

The problem thus formulated contains two implicit parameters: the coefficient of friction C_f and the relative radius R of leading edge curvature. Numerical calculation of the unknown coefficients a_{11}, a_{12}, etc. in (3) was made by the method of descent. In the zero-th order approximation, equation (3) describes pyramids. For a pyramid with a sharp leading edge, calculations show that the larger the span (21), the higher is the aerodynamic quality. At moderate ℓ_1, the quality K of such pyramids and the slope P of the lower surface toward the x axis only weakly depend on ℓ_1 (Fig. 1 and 2). At moderate ℓ_1, the friction T is one third of the total drag.

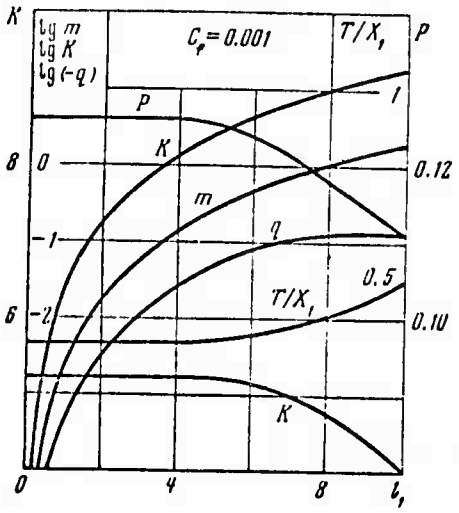

Fig. 1. Maximized parameters of pyramids with sharp leading edges at $C_f = 10^{-3}$.

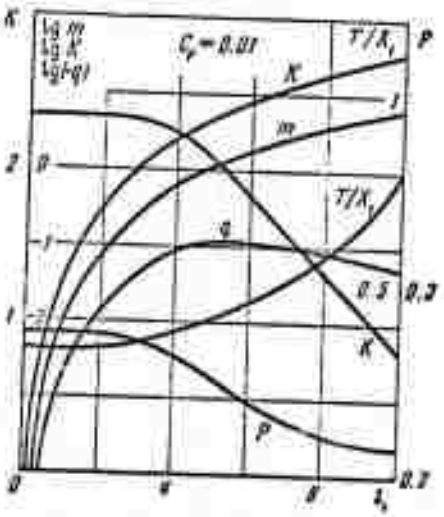

Fig. 2. Maximized parameters of pyramids with sharp leading edges at $C_f = 10^{-2}$.

The effect of bluntness R of the leading edge is primarily evident on ℓ_1 of the optimized pyramids (Fig. 3). The parameter P remains constant over the entire range of R in contrast to the pyramids with sharp leading edges. The leading edge bluntness does not significantly affect the aerodynamic quality of a lifting body. The values of parameters m, ℓ, k calculated from (3) in the first and second approximation indicate that the aerodynamic quality of optimum bodies differs by less than 0.1% from that of the corresponding pyramids. The data are in qualitative and quantitative agreement with the earlier Western data approximating cone-shaped bodies with sharp leading edges.

It is concluded that the geometry of the body type studied, having a given volume and a maximum aerodynamic quality, is nearly pyramidal and in good agreement with the earlier advanced hypothesis.

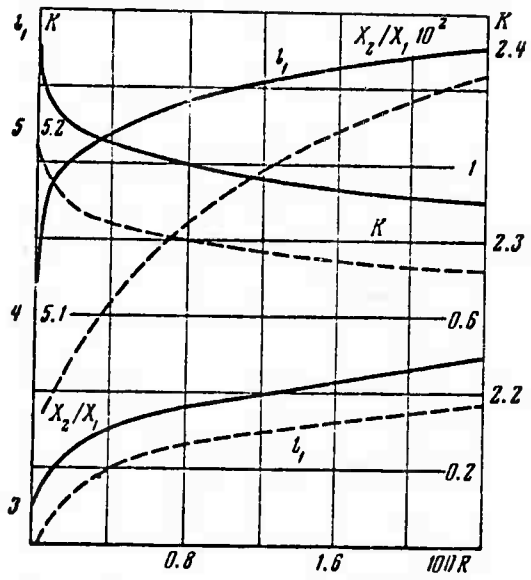

Fig. 3. The parameters of the optimized pyramids versus blunt R. Continuous line - $C_f = 10^{-3}$; broken lines - $C_f = 10^{-2}$.

Temkin, L. A. Approximate solution to the problem of the ground zone in a rarefied gas. MZhiG, no. 1, 1972, 139-143.

Two-dimensional equilibrium flow in a monatomic rarefied gas around a semi-finite rectangular bar is analyzed, on the basis of the Krook model for collision processes in gases. The Krook equation is given in the form

$$f = Vf_0 \tag{1}$$

where $f = f(r, u)$ is the coordinate and velocity distribution function of gas molecules, $f_0(r, u)$ is the local Maxwellian distribution function, and V is the integral kinetic operator. A set of equations

$$n(r) = \iiint_{-\infty}^{+\infty} Vf_0(r, u)\,du, \qquad U(r) = \frac{1}{n(r)} \iiint_{-\infty}^{+\infty} u \cdot Vf_0(r, u)\,du$$

$$T(r) = \frac{m}{3kn(r)} \iiint_{-\infty}^{+\infty} [u - U(r)]^2 Vf_0(r, u)\,du \tag{2}$$

was derived from (1) for gas density n, macroscopic velocity U, and temperature T. The set of equations (2), where k is the Boltzman constant and m is the molecular mass, was solved by iteration in a first-order approximation both with and without allowance for conditions at infinity. Using the M-20 computer, the macroscopic flow parameters n, U, and T were calculated and plotted against coordinates x and y, where the x-axis is the flow direction at infinity. The plots calculated for the Knudsen number $K_\infty = 1$ and Mach number $M_\infty = 2$, and for $K_\infty = 1$ and $M_\infty = 0.75$, displayed a sharp rise in T in the ground zone of the bar, near the corners, followed by a smooth decrease to the T level at infinity. T on the axis of symmetry is maximum at the points $x_\infty \approx 1$ and 0.6 at $M_\infty = 2$ and 0.75, respectively. At both M_∞ values, n and pressure p=nT increase monotonically to the levels at infinity. At $M_\infty = 2$, the stream line deviates from the body near the ground zone because of decelerating gas flow. Results are in qualitative agreement with an earlier solution to the ground zone problem obtained within the framework of the Navier-Stokes equations.

Shapiro, Ye. G. Shock layer radiation during hypersonic air flow around a spherical segment. MZhiG, no. 1, 1972, 101-106.

A theoretical analysis is presented of the effect of shock layer radiation on gas dynamic parameters of hypersonic air flow (V_∞ = 10-16 km/sec) around a spherical segment of a base with radius R. The shock layer flow (Fig. 1) is described by a set of integro-differential

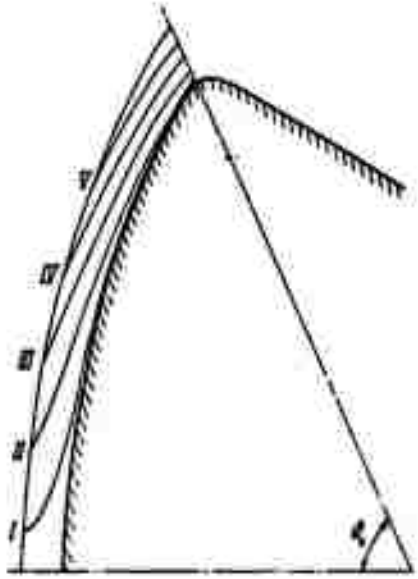

Fig. 1. Shock wave profiles and flow line system for a segment of R = 1 m at V_∞ = 15 km/sec: the flow line numerals I thru V correspond to ϑ = 0.1, 0.3, 0.5, 0.7 and 0.9, respectively.

equations in the spherical coordinate system r, ϑ, whose origin is shifted at a distance l = 0.65 R from the segment center. The term Q or the divergence of the integral radiation flux in the equations was apparently known. The equations were then solved for gas dynamic parameters using an iterative method and an independent variable

$$\xi = (r - r_b)(r_s - r_b)^{-1} \qquad (1)$$

where r_s is the shock wave profile and r_b is the body profile. All gas dynamic parameters and r_s were approximated by Lagrangian polynomials with Hugoniot relations and impermeability as boundary conditions in the shock wave and on the body surface, respectively.

Calculations were made for segments of R = 0-4 m over the cited range of V_∞. In most cases, temperature T_∞ ahead of the shock wave was assumed to be 250°, and in all calculations P_∞ was assumed to be 10^{-4} atm. As with flow around a sphere, the radiation effect on p and V was found to be practically nonexistent and extremely weak with respect to the distribution of the velocity component v. Also analogous to the flow around a sphere, the flow difference with and without radiation was greatest at the body surface. The temperature distribution parameter was the one most affected by shock layer radiation (Fig. 2). The higher the flight speed,

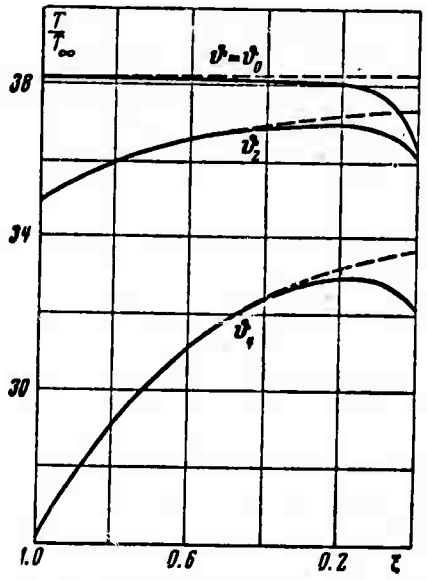

Fig. 2. Relative temperature distribution at V_∞ = 9.85 km/sec, R = 1 m with (solid lines) and without (dashed lines) allowance for radiation flow along the lines ϑ_2 = 0.747, ϑ_4 = 1.141.

the more noticeable was the radiation effect on T distribution. Radiation cooling was also intensified by an increase in R (Fig. 3) The plots in Fig. 2 versus those in Fig. 3 illustrate the effect of the flow velocity around the segment. A decrease in T of the shock layer results in a decrease in

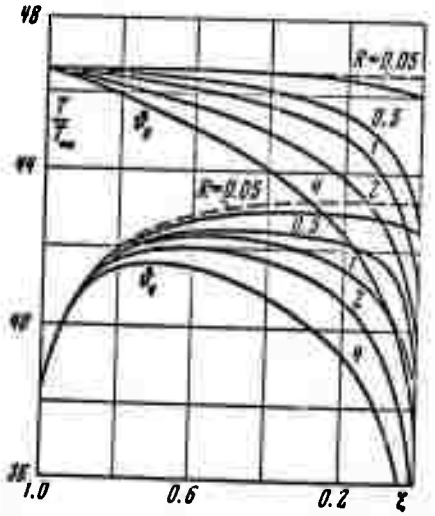

Fig. 3. Relative temperature distribution at V_∞ = 12 km/sec and R = 0.05-4.

layer thickness. It was shown that the radiation energy flux to the stagnation point increases with an increase in R, primarily due to spectral line radiation, in agreement with spectroscopic theory. The universal dependence of the ratio of radiation flux to a body and at the stagnation point is also valid for a spherical segment. An earlier conclusion that the nose of a streamlined body is one area where radiation heating exceeds convective heating applies also to a spherical segment.

The effect of radiation near the rounding point on gas dynamic parameters distribution in a shock layer was also analyzed on the basis of the energy conservation equation. This equation indicates that as $Q \to 0$, the total enthalpy H along different flow lines is even affected by small radiation fluxes (Fig. 4). Fig. 4 illustrates the phenomenon of radiative freezing which occurs when a particle is carried out of the region affected by radiation to a colder region before the particle energy is significantly affected. This phenomenon determines changes in distribution of gas dynamic parameters near the symmetry axis and, in particular, causes a sharp drop of H. In regions far from the symmetry axis, particles propagating along the flow lines do not lose energy because of the high velocity and low Q of radiation

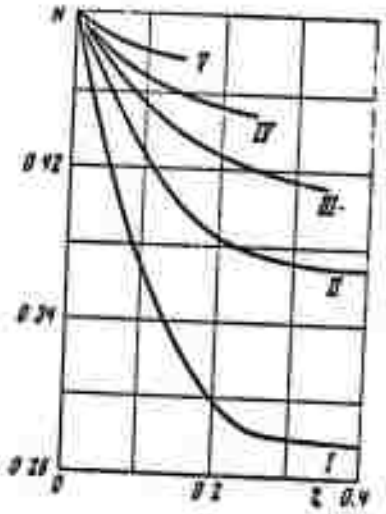

Fig. 4. Distribution of total enthalpy H along different flow lines. ξ is the distance traveled by a particle from the shock wave.

flux. The radiation near the rounding point therefore does not significantly affect distribution of aerodynamic parameters of the shock layer. Calculations showed that allowance for the geometry of the radiative volume is not required in the vicinity of the rounding point.

Avduyevskiy, V. S., V. K. Gretsov, and K. I. Medvedev. Flow stability with leading edge stall zones. MZhiG, no. 1, 1972, 74-81.

Two-dimensional and axisymmetric leading-edge stall zone instability was investigated in both laminar and turbulent gas flow past a semifinite plate with a fixed flat step (Fig. 1a) and around a cone with a fixed shield (Fig. 1b). The free-stream M varied from 2.9 to 6. The combination of a periodically alternating strong expansion and complete

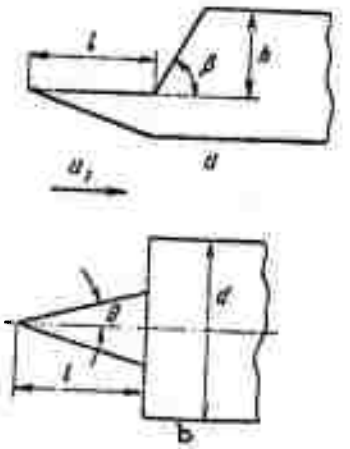

Fig. 1. a - semifinite plate with fixed step of height h and width b; b - cone with a fixed shield of diameter d.

disappearance of stall zones was considered as instability. The geometry effects of the streamline bodies on flow characteristics were studied, i.e., the parameters ℓ, b/h, and β of the plate and ℓ/d and Θ of the cone. Shadow photography and high speed motion pictures were used to record gas flow phases. An unsteady regime with pulsations of compression shock was observed in the flow past the plate when the boundary layer in front of the separation point was either laminar or turbulent. The pulsations disappear at $b \cong h$, $\beta = 70^{\circ}$ or at $\ell < \Delta$, the shock wave separation value in a perfect gas. The flow stabilizes when b/h is decreased.

The flow around the shielded cone, with a surface laminar boundary layer, is steady at a sufficient ℓ, but becomes unsteady when ℓ/d is decreased below a certain value. The flow restabilizes when ℓ is decreased to a value $< \Delta$. Four distinct phases of pulsations were detected in the unsteady flow. The flow is steady at $\Theta > \Theta_*$; Θ_* depends on M of free-stream flow (Fig. 2). Flow stability in region I depends on ℓ/d. In region II, the

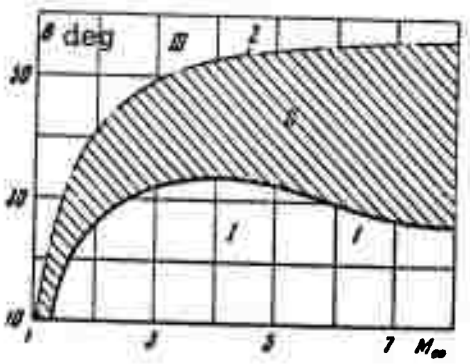

Fig. 2. Angle Θ versus Mach number in free-stream flow. Curve 1 - theoretical Θ_*, 2 - Θ limits of separation.

flow is steady without separation of the turbulent boundary layer, and in region III the shock wave is separated. The value of the angle γ between the plate or cone surfaces and a line connecting the leading edge or cone tip with the upper edge of the step or shield is established as a flow stability criterion. The flow is steady if $\gamma < \gamma_*$, the critical value. The effect of three-dimensional flow transition on pulsations was also evaluated using experimental data.

Kokin, G. A. and Ye. V. Lysenko. Pitot tube pressure in supersonic rarefied gas flow. MZhiG, no. 1, 1972, 195-199.

Readings of four Pitot tubes in a low density wind tunnel at M_∞ = 2.5, 2.6, 3.2, and 5.4 are compared to Pirani and McLeod pressure gauge data. The experiments were designed to evaluate a correction to Pitot tube readings in a supersonic rarefied gas flow. The d/D parameter of the experimental Pitot tubes (Fig. 1) was 0.1-0.2 and 0.5-0.9 for 1, 2 and 3 tube types, and the ℓ/d parameters was 1 and 50-100 for the 1 and 2, 3 types. The mean free path λ_∞ of molecules in a free stream flow was 0.5, 1.2-0.9, 3.3-2.4, and 0.5-0.4 mm, respectively, at the cited M_∞ values. The Knudsen number ($Kn_\infty = \lambda_\infty / D$) dependence on the relative Pitot tube readings at the cited M_∞ is also plotted in Fig. 1, where p_{o*} is the measured Pitot tube pressure and p_{o2} is the Pitot pressure behind the compression shock.

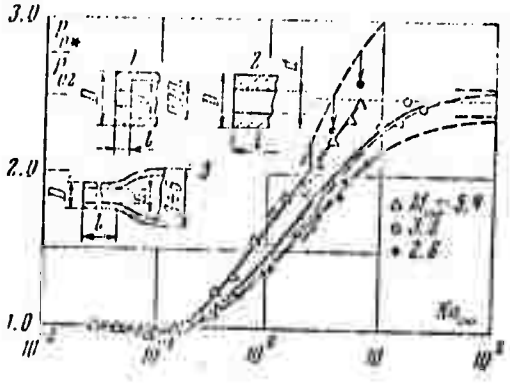

Fig. 1. Geometry of Pitot tubes and experimental plots of P_{o*}/P_{o2} versus Kn_∞. Dotted lines - theoretical plots for r/R = 0.5 or $\simeq$ 0.863. Arrows indicate theoretical values corrected for thermal conductivity of the tube.

To evaluate the correction to the Pitot tube readings, the correction to the Pitot tube readings, the asymptotic pressure ratio p_{oF}/p_{o2} in free molecular flow around the tube was formulated using known relations, including that of Rayleigh. The derived formula served to calculate and plot p_{oF}/p_{o2} ratios for thermally insulated tubes of different ℓ/d parameters and for M_∞ = 1-9. The relation

$$\frac{p_{o*}}{p_{o2}} = \frac{p_{oF}}{p_{o2}}\left(1+\frac{s_\infty}{2\sqrt{2}\,Kn_\infty}\left\{\left[h_1\left(\frac{T_\infty}{T_0}\right)^{1/2}+\frac{h_2}{s_\infty}\right]F(s_\infty)+\right.\right.$$
$$\left.\left.+\frac{h_1 G(s_\infty)}{2s_\infty}\left(\frac{T_\infty}{T_0}\right)^{1/2}\right\}E\left(\frac{r}{R}\right)\right)^{-1}$$
$$h_1=\frac{3\pi-2}{6\sqrt{\pi}},\quad h_2=\frac{2\pi-3}{3\pi},\quad E\left(\frac{r}{R}\right)=\frac{r}{R}+\left[1-\left(\frac{r}{R}\right)^2\right]^{1/2} \qquad (1)$$
$$F(s)=1/2\sqrt{\pi}(1+\operatorname{erf} s)-s\exp(-s^2)$$

was derived for a thermally insulated, long cylindrical tube in a nearly free molecular streamline flow, where $S_\infty = M_\infty / V_\infty$, the ratio between the stream mass velocity and the most probable thermal velocity of molecules; and r and R are the inner and outer radii of the tube. This relation was derived in approximation of a single collision between the incident molecules and those emitted by the tube. The p_{o*}/p_{o2} values for $M_\infty = 2.6$ and 3.2 calculated from (1) are in good agreement with corresponding experimental values (Fig. 1). An additional correction factor C for thermal conductivity was introduced into (1) to obtain theoretical p_{o*}/p_{o2} values at $M_\infty = 5.4$ in agreement with the experimental data. The experimental and theoretical data were used to plot a universal Kn dependence of the parameter $\xi = (p_{o*}-p_{o2})(p_{oF}-p_{o2})^{-1}$, independent of M_∞. The plot can then be used to determine M_∞ from measured Pitot tube pressure.

Stulov, V. P. Strong blowoff on a blunt body surface in supersonic flow. MZhiG, no. 2, 1972, 89-97.

A theoretical analysis is made of the supersonic axisymmetrical flow of a perfect gas around a blunt body, with simultaneous injection of another gas through the body surface according to a specified formula. The incoming gas passes through shock wave S and spreads along the contact surface C with the injected gas (Fig. 1). The two-layer flow is described by a set of gas dynamic equations with boundary conditions in the shock wave, at the C and body surfaces. The equations are formulated in a system of spherical coordinates ξ, θ centered on the flow axis, and are solved separately for each layer assuming that the pressure on the C outer side is given by the Newton formula

$$p_{1c} = p_1^* \sin^2 \sigma \qquad (1)$$

where σ is the angle of the flow axis with C. A complete numerical solution of the boundary problem by the method of successive approximation is given for injection according to the formula

$$u_w = u_{w_0} \cos^n \theta \qquad (2)$$

which describes the distribution of the radial component of injection velocity over the front surface in a hypersonic flow, e.g., $M_\infty = 10$, around a spherical body with r_c radius (Fig. 1). The discrepancy between the approximate

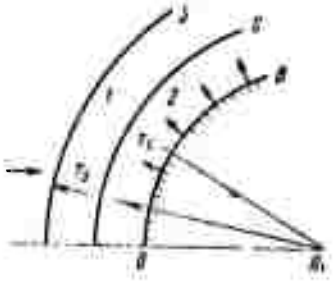

Fig. 1. Flow diagram around a blunt body B with injection:
1- shock layer, 2- injected gas layer

and exact numerical solution for layer 2 is shown to be insignificant. Two approximate analytical solution variants for layer 2 are presented. One variant is based on an assumption of constant but different densities of the 1 and 2 layers. In this case, two equations are solved for r_s and r_c. The solution for layer 1 approximates well the numerical data calculated earlier by the author for a flow around different bodies. The solution for layer 2 near or far from the symmetry axis agrees with the approximate numerical solution. The other solution variant for layer 2 was obtained within the framework of boundary layer approximation and local flow self-similarity. The solution in this case agrees with the first variant near the flow axis and at small values of the ratio K of specific kinetic energy of injection and incoming flows. But the discrepancy with numerical solution becomes significant at a distance from the axis, e.g. ~20%.

Mikhaylov, V. N., and V. S. Tamilov. Supersonic flow over an edge formed by intersecting plates. MZhiG, no. 2, 1972, 162-166.

A mathematical method is introduced for the numerical solution of a supersonic flow problem on the edge formed by two perpendicular plates of zero thickness. In a Cartesian coordinate system, the plates are made to coincide with the $y = 0$ and $z = 0$ planes, and the velocity vector V_∞ is defined by the angle of attack α and the angle θ between the y-axis and the projection of V_∞ on the $x = 0$ plane (Fig. 1). Pressure p, density ρ, and the velocity components u, v, w must satisfy a set of differential equations with plate boundary conditions. Solution of the equations is obtained in the region bounded by the $y = 1$, $z = 1$, and $x \geq 0$ planes using the method of adjustment. Formulas are given for the flow parameters u, v, w, ρ, and p and the stability condition of the calculation scheme.

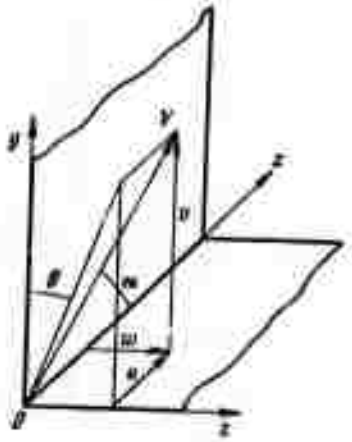

Fig. 1. Flow diagram over the edge in perpendicular plates

Plots of the calculated parameters along the half-lines $y/x = \text{const}$ ("conical" variable) show that the parameters become constant at high x values (Fig. 2). A qualitative theoretical flow pattern plotted for a perfect gas presents shock wave traces as flow region boundaries with sharply different parameters. It is concluded that the perfect gas model is inadequate to describe the flow type studied, because of a discrepancy between the pattern and an earlier experimental pattern of interference flow over an edge in intersecting wedges. The method of calculation was also applied to the expansion flow between two perpendicular plates. Calculations at $M_\infty = 6$, $\theta = 45^\circ$, $\alpha = 10^\circ$ show that flow ahead of the interference region is directed from the edge with a subsequent significant decrease in p in the interference region.

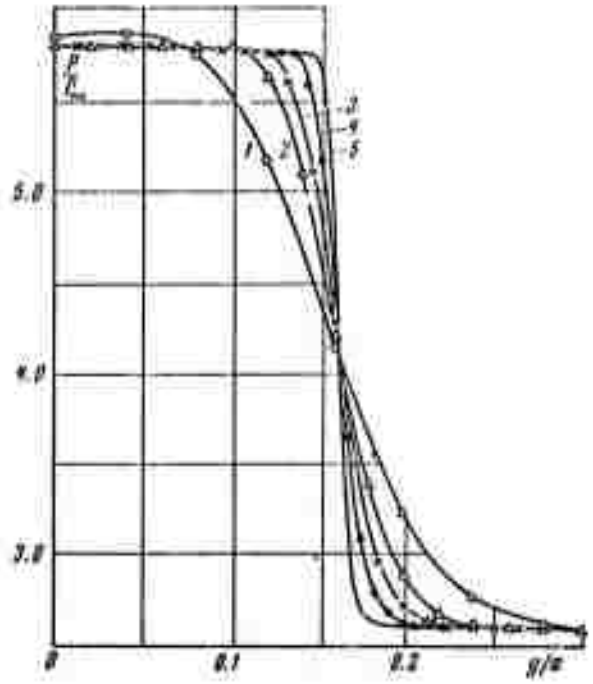

Fig. 2. Typical plot of p distribution along the y axis for the parameters $M_\infty = 6$, $\theta = 45^\circ$, $\alpha = -10^\circ$ of the incoming flow. The curves 1, 2, 3, 4, 5 correspond to increasing x values

V. ATMOSPHERIC PHYSICS

Bykov, B. P., and S. I. Kozlov. Ion and electron kinetics in a disturbed ionosphere at altitudes of 100~200 km. Geomagnetizm i aeronomiya, no. 2, 1972, 340-342.

Results are described of an investigation on kinetics of ions and electrons at altitudes $100 < h < 200$ km in a disturbed atmosphere. The disturbing action is assumed to significantly increase the degree of ionization α of air, so that N_2^+, O_2^+ and O^+ are formed approximately in direct relation to the N_2, O_2 and O contents at these altitudes. Investigation is limited to values $\alpha \ll 1$, so it is considered that the atmosphere is not warmed up due to a sharp rise of α, i.e. electrons, neutrons and ions of gas have the high level of temperature distribution existing in normal ionosphere.

Form. no.	Reaction	Velocity const × cm^3 per sec
1	$O^+ + N_2 \rightarrow NO^+ + N$	$\alpha_1 = 2 \cdot 10^{-12}$
2	$O^+ + O_2 \rightarrow O_2^+ + O$	$\alpha_2 = 4 \cdot 10^{-11}$
3	$N_2^+ + O \rightarrow O^+ + N_2$	$\alpha_3 < 1 \cdot 10^{-11}$
4	$N_2^+ + O \rightarrow NO^+ + N$	$\alpha_4 = 2{,}5 \cdot 10^{-10}$
5	$N_2^+ + O_2 \rightarrow O_2^+ + N_2$	$\alpha_5 = 1 \cdot 10^{-10}$
6	$O_2^+ + N_2 \rightarrow NO^+ + NO$	$\alpha_6 < 1 \cdot 10^{-15}$
7	$O_2^+ + e \rightarrow O + O$	$\alpha^*(O_2^+) = 2{,}2 \cdot 10^{-7} (T_e/300)^{-1}$
8	$N_2^+ + e \rightarrow N + N$	$\alpha^*(N_2^+) = 3 \cdot 10^{-7} (T_e/300)^{-0.5}$
9	$NO^+ + e \rightarrow N + O$	$\alpha^*(NO^+) = 4{,}4 \cdot 10^{-7} (T_e/300)^{-1}$, $200^\circ K \leqslant T_e \leqslant 500^\circ K$
		$\alpha^*(NO^+) = 0{,}9 \cdot 10^{-7} (T_e/1000)^{-0.5}$, $T_e > 500^\circ K$

Table 1.

The general scheme of elementary processes used in this work and their velocity constants are given in Table 1. On the basis of these reactions kinetic differential equations are obtained which were solved by computer. Calculations are done for a wide range of altitudes and values of N_{eo}, at day and night conditions. Results of calculations for daylight conditions at $\alpha_3 = 10^{-11}$ and $\alpha_6 = 10^{-15}$ cm^3/sec are plotted. The main characteristic features of ion and electron kinetics in a disturbed ionosphere are seen to be as follows: 1) The role of N_2^+ ions is significant only at the initial moment after disturbance, not exceeding in most cases ~1 sec;

2) At lower altitudes, as in a normal atmosphere, recombination takes place mainly according to a square law. However, with an increase of N_{eo} after the disappearance of N_2^+ over a certain time, velocity variation may follow a linear law. The duration of this time significantly increases at higher altitudes; 3) The time behavior of $[NO^+]$ differs little from predictions. Even at upper altitude regions, the role of this ion is small, except when $N_{eo} < 10^6$ cm^{-3}; 4) To a first approximation, at all altitudes the main molecular ion is O_2^+; 5) The principal difference in behavior of ions and electrons in night conditions from day consists in the fact that the dissociative recombination level increases, so that the role of N_2^+ and NO^+ ions substantially decreases; and 6) The decay time of electron concentration from N_{eo} to normal values of an undisturbed ionosphere has only a slight dependence on the value of N_{eo}.

These conclusions also hold up under varying values of the unknown velocity constants α_3 and α_6. All calculations were done assuming $\alpha_1 - \alpha_6$ to be independent of temperature.

Alimov, V. A., L. M. Yerukhimov, and T. S. Pyrkova. Theory of the F_{spread} phenomenon in the ionosphere. Geomagnetizm i aeronomiya, no. 5, 1971, 790-797.

An analysis is given of possible factors which cause stretching of the return r-f pulse from an ionospheric probe, or the F_{spread} effect. The authors use the diffraction theory of pulsed signal spread in a nonuniform ionosphere, together with data on nonuniformity distribution vs. altitude in the F-layer, and diffusivity data on returned signals. Both ground-based and satellite transmitters are considered, and the variation in spread effect at different latitudes is considered. Using an averaged model of the F-layer structure, the authors obtain expressions for electron density variation $\Delta N/N$ in the equatorial, middle and high latitudes. Following this the characteristic of returned pulsewidth τ is obtained for several possible $\Delta N/N$ models, assuming either an exponential or parabolic variation within a layer, as tabulated in Table 1. Graphical comparisons are given of theoretical and calculated behavior of the depth of the diffusivity zone $\Delta z \equiv c\tau$ as a function of signal frequency. Fig. 1 gives this relation for the extremes of equatorial and polar latitudes, based on ionogram data from the Alouette satellite. These

Model of non-uniform layer	Exponential layer	Parabolic layer
$\overline{(\Delta N)^2}(z) = \text{const}$	$\tau \sim \omega^{-2}$	$\tau \sim \omega$
$\overline{(\Delta N/N)^2}(z) = \text{const}$	$\tau \approx \text{const}$	$\tau \sim \omega^2$
$\overline{(\Delta N)^2}(z) = B/A - z$	—	$\tau \approx \text{const}$
$\overline{(\Delta N/N)^2}(z) = A_1 e^{-\alpha z}$	$\tau \sim \omega$	—
$\overline{(\Delta N/N)^2}(z) = C_1 + B_1 e^{\alpha z}$	$\tau \sim \sqrt{C_1 + B_1/\omega^2}$	—

Table 1.

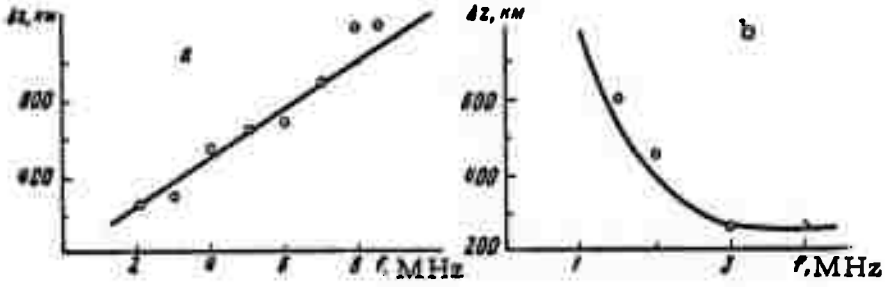

Fig. 1. $\Delta z(f)$ for satellite signals.
a - equatorial, b - polar latitudes

results show a distinct variance from analogous data using a ground-based probe system, as seen in Fig. 2, indicating the discrete nature of inhomogeneities in differing portions of the F-layer. The findings appear to

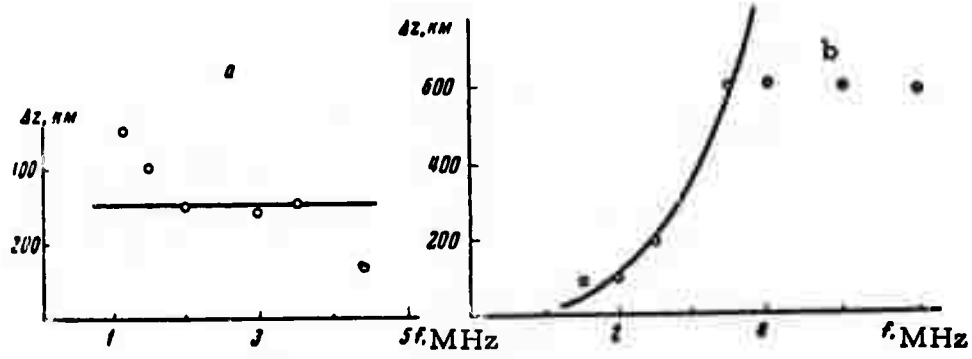

Fig. 2. $\Delta z(f)$ for ground-based signals.
a - equatorial, b - polar latitudes

establish that the F_{spread} mechanism is generally caused by scattering of the signal pulse on local electron density variations in areas on the order of 1--5 km across. The variation in spread behavior is then governed by the noncorrelation in spectral response of the pulse, as it is reflected from different levels of the F-layer.

Alimov, V. A. Frequency correlation of fluctuations in radiowaves reflected from the ionosphere. Geomagnetizm i aeronomiya, no. 3, 1972, 548-551.

The author considers the question of frequency correlation in the received fluctuations of dual frequency waves reflected from the ionosphere, as a means of interpreting some inhomogeneous characteristics of the ionosphere. As noted previously, the correlation function $R(f_{\omega_1} f_{\omega_2}^*)$ may vary both within the ionosphere and beyond it; also vertical refraction effects must be allowed for. Alimov analyzes the general case of inclined incidence of the transmitted beam, and determines expressions for $R(f_{\omega_1} f_{\omega_2}^*)$ at varying conditions of ionospheric anisotropy. Analysis of this case generally requires calculation of the trajectories of wave normals when a substantial effect of vertical refraction on $R(f_{\omega_1} f_{\omega_2})$ is to be expected.

Vul'fson, N. I., and L. M. Levin. Explosive breakup of developing cumulus clouds. FAiO, no. 2, 1972, 156-166.

Upward and downward spontaneous convective jets initiated by explosions at various heights in developing cumulus clouds were investigated. Relationships are found among the parameters of jets formed in different sectors of an unstable layer (a conventional developing cumulus) to determine those zones in which explosions create significantly more intensive downward rather than upward movements. Mathematical expressions are derived and results are tabulated. Comparison of the calculated jet velocities shows that explosions in the upper sectors of developing cumulus produce a system of spontaneous jets, with a destructive capacity (caused by the downward jets) considerably exceeding the intensity of cloud development, due to upward jets. The more favorable the condition of cloud development, the greater the intensity of cloud destruction. Experiments were conducted under natural conditions in the Fergansk valley during May 1970, using explosive shells in dense convective clouds. The shooting of two cumulus, 5500 and 6600 m thick, by antiaircraft mine shells lowered their thickness by 3 to 4 times and the clouds gradually vanished. The explosion effectiveness can be further increased by blasting with a special type of cumulative shell, which generates downward jets during explosion.

VI. SOIL MECHANICS

Iskakbayev, A. Crack propagation in the curve of a linear viscoelastic fold. VAN KazSSR, no. 12, 1971, 54-57.

Brittle fracture of a viscoelastic layer (rectangular band) compressed at the ends by a force p within a fold of a rock mass is analyzed. The fracture is examined as a jointing process with a creep deformation background. The material of the rock mass is described by the standard linear body model. The time required for fracture initiation is determined from a formula of tensile stress in the curved section of a fold subjected to a bending force (p-q), where q is the weight of the rock mass. Solution of a transcendental equation gives the time $t > t_1$ necessary for fracture propagation through a 2δ thick layer cross section from a given point of the surface fiber. Determination of the time of layer fracture is similarly arrived at when the layers are described by a Maxwellian model.

Rodionov, V. N., V. V Adushkin, V. N. Kostyuchenko, V. N. Nikolayevskiy, A. N. Romashov, and V. M. Tsvetkov. The mechanical effect of an underground explosion. Moskva, Izd-vo Nedra, 1971, 224 p.

A comprehensive review is given of all fundamental characteristics relating to mechanical effects of underground explosions. A simplified method is set forth for calculating explosion-produced mechanical motion, which enables prediction of explosion cavity dimensions, destruction range, fissurability of rock, parameters of cratering explosions, and intensity of seismic waves. Theoretical results are compared with experimental laboratory and field data from Soviet and non-Soviet sources. Engineering applications of strong underground explosions are discussed; examples given include the creep dam against mud-debris flows formed in Medeo, near Alma-Ata, in 1966-67, and the Baypazinsk explosion of 1968 which generated a rock slide to dam the Vakhsh River. Theoretical solutions to analogous problems are included, using basic physical properties of soil and rock, and possible future developments in the techniques are suggested.

VII. LASER SIMULATION AND RELATED EFFECTS

Ashmarin, I. I., Yu. A. Bykovskiy, V. A. Gridin, V. F. Yelesin, A. I. Larkin, and I. P. Sipaylo. Shock waves generated by the action of laser radiation on transparent bodies. IN: Sbornik. Kvantovaya elektronika. Moskva, Izd-vo Sovetskoye radio, no. 6, 1971, 126-128.

A set of experiments is described on interaction of powerful laser radiation with type K-8 glass, with the object of determining the criteria for shock wave generation at the focal point. A Q-switched ruby was used generating 50 Mw pulses, focused to a 0.2 mm spot both internally and on the glass surface. A holographic plus high-speed framing method was used to determine wave propagation velocity. Results confirmed that the transition from a longitudinal sonic wave to a shock wave generally occurred near the damage threshold. Wave velocity was observed to be a function of pulse intensity, as well as of delay time in pulse application, as seen in Fig. 1. In theory the sonic wave converts to a shock wave when

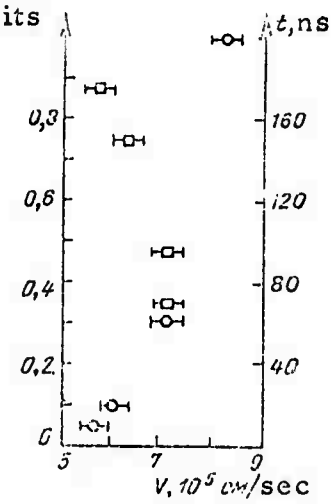

Fig. 1. Wave velocity vs. delay (squares) and laser pulse intensity (circles).

pressure p in the focal region attains a value of $\rho_o C_o^2$, where ρ_o is glass density and C_o is the sonic velocity in the glass. A sample calculation based

on actual parameters was made on this assumption, showing that shock wave velocity should be 1.3 times sonic; this agreed closely with measured results. With the beam focused on the surface a dual spherical wave was typically generated, as shown in Fig. 2. Their characteristics were essentially the same as for the internally focused pulse.

Fig. 2. Dual wave generation from surface irradiation.

Cherkun, Yu. P., and I. N. Konopel'ko.
Current status of experimental and theoretical studies in the field of combined heat exchange.
I-FZh, v. 22, no. 4, 1972, 757-758.

A brief summary is given of several papers on the subject of radiation - induced heat exchange, presented at a session of a general conference on mass and heat transfer held on Sept. 15-17, 1971 at the Thermophysics Institute, Siberian Branch AN SSSR. The general theme of the session was phenomena related to combination heat transfer mechanisms, namely radiative - conductive and radiative - convective.

S. S. Kutateladze and D. I. Avaliani reported on experimental findings of laser beam attenuation in liquid media with pulsating turbulence; this work was judged important from a heat transfer viewpoint as well as in regard to beam propagation in a turbulent medium. A related paper by V. M. Kostylev and V. Ya. Belostotskaya dealt with the relation between conductive and radiative heat transfer in optically thin layers of finely-dispersed media; they show that in this case it is incorrect to use the hypothesis of additive fluxes.

A report by N. A. Rubtsova and A. E. Berte covered the thermal state of pure metal surfaces exposed to a constant thermal flux. Results showed anomalies in surface temperature distribution (the Jacques

effect) on metals including Al, Fe, Sn and others; several possible models for this phenomenon are advanced.

V. M. Yeroshenko discussed variants of ablation techniques in which blowoff of dispersed media is used as a protection against radiative flux; this refers to processes at levels of 100 atm and temperatures in the 20,000°C range. Several papers by other authors dealt with heat exchange studies in various types of combustion reactions.

Special mention is given to a paper by A. I. Leont'yev and A. M. Pavlyuchenko which is cited as giving the most complete picture to date on temperature distribution in a turbulent boundary layer and laminar sublayer in a thermal radiation field. As with Kostylev et al, these authors also demonstrate the fallacy of the additive-flux hypothesis under their test conditions.

In closing, S. Kutateladze stressed the need for further experimental data on radiative heat exchange resulting from interaction of e-m waves with materials.

Epshteyn, E. M. Thermal instability of a semiconductor in a laser beam. IVUZ Radiofiz, no. 1, 1972, 33-37.

A theoretical study is presented on a possible mechanism of laser-induced destruction of a semiconductor. The case is limited to photon energies less than the width of the forbidden zone, so that the main exchange mechanism is absorption by free carriers. In the general case a cumulative heating and increase in free carriers will occur, resulting in a stationary temperature field. However, above some laser threshold level the stationary field breaks down and a rapid thermal reaction sets in which is analogous to breakdown in a d-c field, or the thermal explosion from an exothermic chemical reaction. To examine the governing phenomena the author assumes the simplest case of a cylindrical semiconductor target, axially excited by a uniform-intensity laser beam such that $\lambda \ll \rho \ll R$, where λ is laser wavelength, and ρ and R are beam and cylinder radii. Expressions are derived for the limit conditions of the stationary field solution, and the corresponding threshold power of the laser is determined. Finally, it is shown that the elapsed time required to reach threshold under practical conditions will lie in the 1 millisec - 1 sec range - i.e. demanding in effect a c-w laser regime. Therefore the described mechanism cannot account for breakdown observed, for example, in transparent dielectrics under nanosecond pulse exposure.

Frolov, V. V. Temperature fields in multilayer translucent coatings under conditions of pulsed radiation heating. I-FZh, v. 22, no. 4, 1972, 755-756. (Annotation of deposited paper.)

A summary is given of an analysis of heat transfer in a multilayer coating system under beamed irradiation. The problem is treated as nonstationary and one-dimensional, with distribution of absorption taken into account. Reflection and concentrated absorption at layer interfaces are treated; the absorption process is considered to be linear.

As an example the temperature distribution is calculated in a two-layer heat shield in which the heat load is assumed to be applied in triangular pulses of a given energy, at durations ranging from 10 to 60 seconds. Owing to changing boundary conditions, it is shown that the system must be solved as a class of piecewise-discontinuous functions. On this basis graphical solutions are obtained showing the time characteristic of heat absorption as a function of absorption coefficient and pulse duration. Instantaneous temperature distributions are also presented for the cases of absolutely opaque as well as semitransparent coating systems.

The analysis shows that failure to account properly for internal heat absorption can lead to significant errors in theoretical temperature fields and level of total absorption; furthermore, the error increases with reduction in pulse width.

Bessarab, Ya. Ya., Yu. B. Tkach, V. P. Zeydlits, N. P. Gadetskiy, and V. V. Dyatlova. Study of collective processes in a plasma using light of stimulated emission. ZhETF, v. 62, no. 2, 1972, 569-572.

The use of coherent light emission to study the collective processes in a plasma-beam discharge is described. It is shown that an effective method of studying these processes is the direct observation of the form of oscillation in the intensity of spontaneous-emission spectral lines, with a subsequent application of Fourier analysis. Study of the oscillation spectrum was performed through investigation of the fluctuation intensity of coherent emission in the Ar II transitions $4p^2D^0_{5/2} \rightarrow 4s^2P_{3/2}$ at a wavelength of 4880 Å, and $4p^4D^0_{5/2} \rightarrow 4s^2P_{3/2}$ at a wavelength of 5145 Å. The maximum frequency excited in the plasma, which depends upon modulation of the

emission intensity, is determined by the relationship $\omega_{max}\tau \lesssim 1$ where τ is the lifetime at the upper level of the observed transition. In this study $\omega_{max} \approx 100\text{-}120$ MHz. In the case of coherent emission, the spectrum of the oscillation being investigated has a lower limit given by

$$\omega_{min} \approx \frac{2\varepsilon_0 E^2 c(1-R)}{(N_1-N_2)\hbar\omega_{12}d},$$

where ϵ_0 is the dielectric permeability of the active medium, E is the field intensity of the light wave in the resonator, c is the speed of light, R is the reflection coefficient of the resonator mirrors, d is the distance between mirrors, $\hbar$ is Planck's constant, ω_{12} is the frequency of the observed transition and N_1 and N_2 the corresponding population densities of the upper and lower laser levels, respectively. Fig. 1 compares obtained spectra of coherent and spontaneous emission.

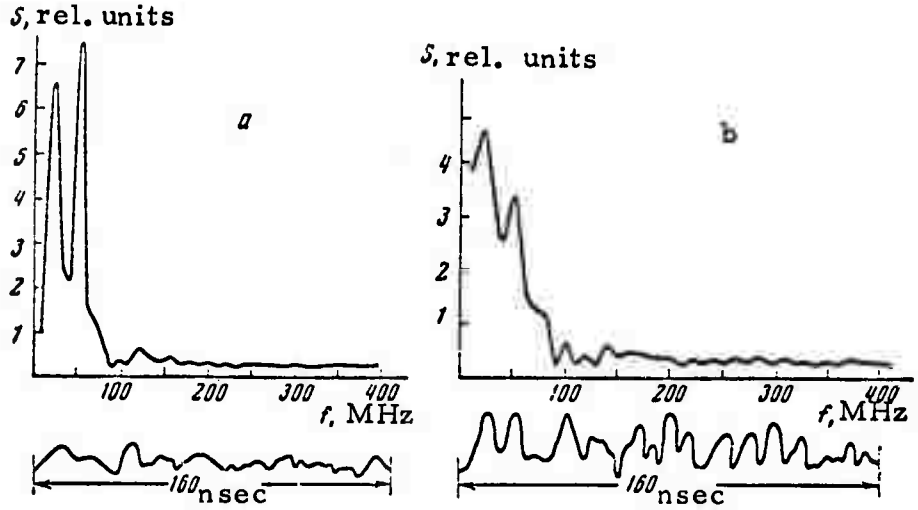

Fig. 1. Realization and type of spectrum obtained. a - by modulation of coherent emission, b - by modulation of spontaneous emission.

Sultanov, M. A. Destruction of transparent dielectrics under the action of free-running neodymium and ruby lasers. Mekhanika polimerov, no. 2, 1972, 359-360.

The author notes that a variety of theories exist on the basic destruction mechanism of laser interaction with transparent solids; among these are thermal explosion, acoustic phonons from stimulated Brillouin scattering, and photolysis of the target material. Experiments are described

which were designed to clarify the predominant mechanism of laser damage in several dielectrics, including polymethyl-methacrylate, polystyrene and several types of glass. Both ruby and neodymium crystal lasers were used, in free-running regimes at energies of 3 to 15 j. Characteristic platelets of cracks at angles up to 90° from the beam axis were observed for both laser types; however in the Nd target specimens the damage area was more extended along the beam axis, whereas the ruby damage was localized near the beam focus. (Repeated reference is made to damage photos, which are unfortunately omitted from the text.)

The test results lead Sultanov to the following concept of the damage process. On focusing a sufficiently powerful beam in the transparent dielectric, a local region is heated to a liquid state in which further energy is absorbed by inhomogeneities, and crack propagation begins. A plasma is generated which expands at high velocity; thus the effect is that of a powerful, instantaneous point explosion. The process is a hydrodynamic one, including shock wave generation which causes further destruction both before and behind the beam focal point. Examples of remote damage regimes in PMMA specimens are cited in added support of the theoretical model.

Korotin, A. V., and L. P. Semenov. Vaporization of crystals under the effect of external excitation. IN: Institut eksperimental'noy meteorologii. Trudy, vyp. 30. Fizika aerodispersnykh sistem. Moskovskoye otdeleniye gidrometeoizdata, Moskva, 1972, 65-71.

The authors present a straightforward thermodynamic analysis of the interaction of a concentrated heat flux with a crystal surface, for the case in which an appreciable melt zone appears prior to evaporation. The analysis assumes a constant-intensity beam normal to a semiinfinite crystal face, and arrives at expressions for melt zone boundaries, growth rate and limit conditions, and time to melt, in terms of target and beam parameters. It is shown that in the general case the maximum temperature will occur at the outer melt surface, and also that an optimum beam intensity exists for which the melt area will be maximum, decreasing at higher or lower intensities. It is interesting to note that the numerical examples given assume an ice target; results on the ice-water parameters are given for beam densities ranging from 25 to 200 w/cm^2. In ice, for example, the depth of the melt zone is only weakly dependent on beam intensity.

Basov, N. G., Yu. S. Ivanov, O. N. Krokhin, Yu. A. Mikhaylov, G. V. Sklizkov, and S. I. Fedotov. Generation of neutrons from spherical irradiation of a target by powerful laser radiation. ZhETF P, v. 15, no. 10, 1972, 589-591.

The authors note some limitations to neutron production from laser heating of a target for fusion purposes. Specifically, the effect of an increasingly powerful focused laser becomes offset by diffusion of the high temperature region owing to thermoconductive and gasdynamic energy loss. An alternative approach suggested recently by Basov et al is to heat a spherical target simultaneously with multiple beams; in the present case this was done with a deuterated polyethylene target exposed to nine equal beams, as indicated in Fig. 1, using an Nd glass laser in the giant pulse

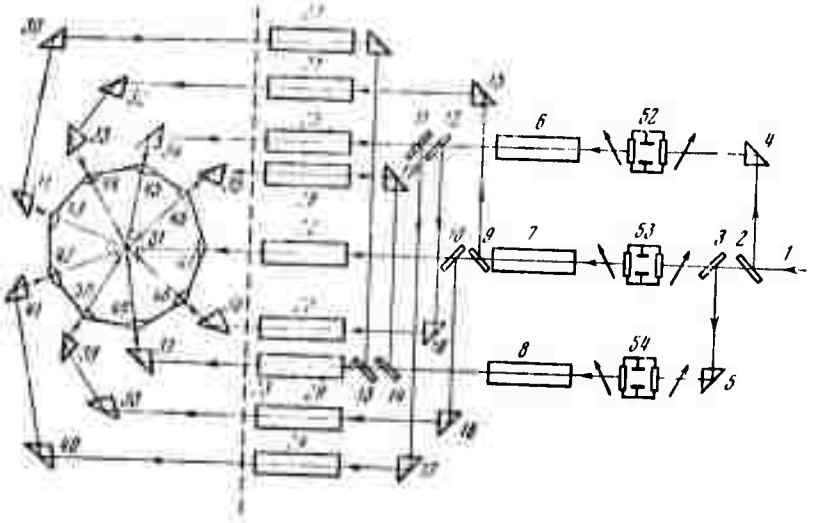

Fig. 1. Multibeam array for CTR target.
1- preamplified beam
6-8- second amplifier
21-29- third amplifier
42-50- focus lenses
Compensating delays for differing path lengths not shown.

mode. This array attained a mean power density of 10^{16} w/cm^2 on the target surface, at 2--16 ns duration. The focusing objectives were placed to obtain a focal plane 200μ from the target, for minimum reflection and uniform heating.

Some results are shown in Table I for various target sizes and beam energies; the measured value was obtained from three scintillation counters. The $n\tau$ values, calculated independently for thermoconductive and gas dynamic regimes, were 2.4×10^{12} and 2×10^{11} respectively. The effect of cumulation in the cited experiments is concluded to be a minor one.

Target radius, cm	Laser energy, j	Mean temp., ev	Neutron output per pulse	
			exp.	calc.
$2{,}50 \cdot 10^{-2}$	600	40	–	–
$1{,}25 \cdot 10^{-2}$	202	120	–	10^2
$5{,}50 \cdot 10^{-3}$	214	840	$3 \cdot 10^6$	$8 \cdot 10^7$
$3{,}00 \cdot 10^{-3}$	232	$4 \cdot 10^3$	–	$1 \cdot 10^{10}$

Table I

Novikov, N. P., and A. A. Kholodilov. Destruction of thermoplastics by the combined action of gas and powerful thermal flux. I-FZh, v. 22, no. 4, 1972, 618-626.

This paper is a repeated treatment of an experiment reported by the authors previously (Effects of High Power Lasers, Dec. 1971, 48), in which the destruction characteristics of several polymers are compared under combined laser and hot gas impact. In the present case only PMMA and polystyrene specimens were used; surface heating was provided by a CO_2 laser plus a coaxial high-speed flow of heated nitrogen over the specimen. The gas jet diameter was more than double the specimen diameter so that the process could be treated as one-dimensional and stationary. The resulting liquefaction, cavity formation and ejection rate of material are discussed as functions of beam power density and jet velocity; the conclusions are as stated in the cited earlier work. The main emphasis is on the differences in destruction characteristics which depend on the chemical structure of the target material. Thus polystyrene shows a monotonic rise in destruction rate with beam intensity and gas velocity, whereas PMMA may show a definite peak in destruction rate for the same heating, as seen in Fig. 1. This is evidently caused by a temporary shielding effect by ejecta in PMMA for two of the four curves in Fig. 1(a), which dissipates at higher gas velocities; no similar effect was found for polystyrene. Rough calculations were also made of the amount of ablated material for the polystyrene target, as a function of beam intensity and flow rate. An extensive theoretical analysis of the observed destruction mechanisms is included.

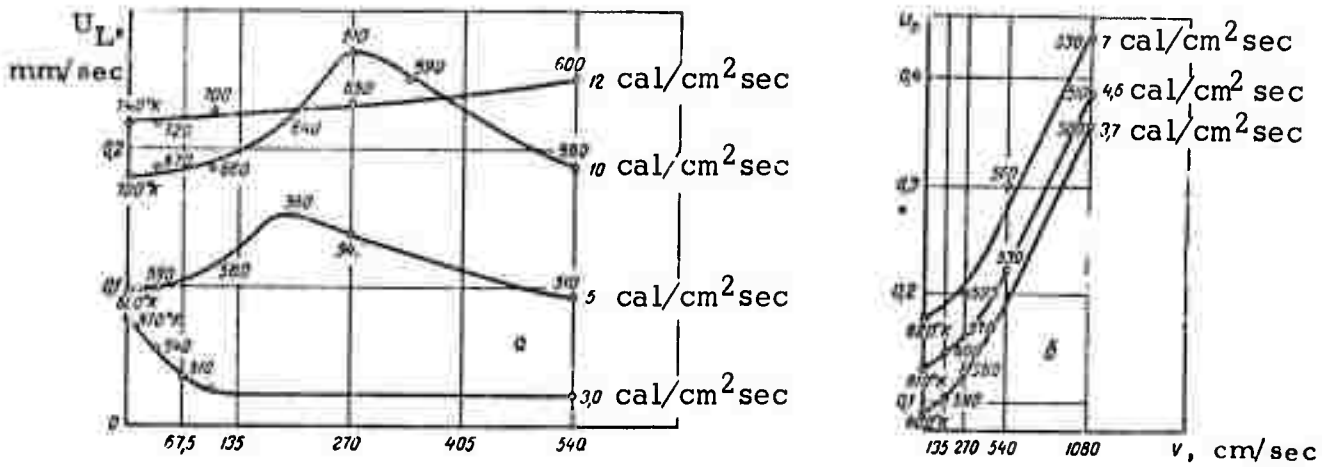

Fig. 1. Linear destruction rate U_L as a function of laser intensity and gas velocity.
a- PMMA
b- polystyrene
Surface temperatures are shown on each curve.

Krasyuk, I. K., and P. P. Pashinin. Breakdown in argon and nitrogen from a picosecond laser pulse at 0.35 micron wavelength. ZhETF P, v. 15, no. 8, 1972, 471-473.

Optical breakdown triggered in Ar and N_2 by the second harmonic emission from a ruby laser was studied to ascertain the breakdown mechanism from 30-50 psec. pulses at 0.35μ wavelength. Breakdown threshold I_{th} was measured in the gases at a pressure in the 400-4500 torr range in an experimental arrangement analogous to one described by the authors and A. M. Prokhorov (ZhETF P, v. 9, 1969, 581). The power of the filtered second harmonic emission was measured with a resolution equal to or better than 20 psec. The emission peak corresponding to the limit of visibility was assumed to be I_{th}. The experimental plots (Fig. 1) indicate that breakdown is triggered by multi-photon ionization of gas atoms or molecules. This mechanism is confirmed by experimental data obtained by the authors and A. M. Prokhorov (ZhETF, v. 58, 1970, 1606) at 0.69μ wavelength. Analysis of the cited data and that of other authors reveals that the quasiclassic formula derived by Keldysh adequately describes the relative decrease in I_{th}, i.e., the increased probability of photoionization, with the increases in frequency of optical emission. In contrast, no theory exists to explain the fact that I_{th} in Ar and Xe also decreases when the breakdown is triggered by a 20 nsec laser pulse at the 0.35μ wavelength; accepted avalanching theory predicts instead a monotonic rise in I_{th} with laser frequency in the nanosecond case. Hence different breakdown mechanisms must be considered in the picosecond and nanosecond pulse cases.

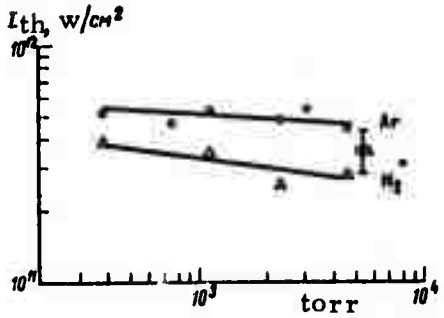

Fig. 1. Experimental plots of I_{th} vs. pressure: o- in argon, Δ - in nitrogen

Kostylev, V. M., and N. V. Komarovskaya. Energy transfer in a medium of low optical density. I-FZh, v. 22, no. 5, 1972, 907-912.

An experimental study was made of the radiative energy transfer in optically thin loose fibrous layers bound by diffusely radiant and reflecting surfaces. Allowance was made for the effects of induced radiation and scattering from the medium in approximation of local thermodynamic equilibrium. The fibrous layers were made of a superthin (1-2μ) fiberglass or ~30μ thick caprone fibers bound by oxidized aluminum and copper or polished aluminum surfaces. The effective thermal conductivity λ_τ of the plane-parallel optically thin layers was measured in an electric calorimeter with a special heat-insulating shield in high vacuum. The maximum λ_τ error was 5%. The experimental λ_τ data are plotted in Fig. 1 in comparison with the theoretical $\lambda_\tau(\tau)$ dependence calculated from

$$\lambda_\tau = \frac{1}{\frac{1}{\lambda} + \frac{1}{4\varepsilon_r \sigma T^3 L}} \qquad (1)$$

where λ is the radiative thermal conductivity of an optically dense layer, σ is the Stefan-Boltzmann constant, T is the arithmetic mean of the layer temperature, L is the geometric thickness of the layer, and ε_r is the reduced emissivity of the boundary surfaces, which was experimentally measured in the absence of the loose fibrous layer. Allowance was made, when calculating λ_τ, for the coefficient $\bar{\mu} = 3/2$ of angular distribution of radiation flux intensity incident on the boundaries. The experimental and theoretical λ_τ/λ versus τ plots for two different ε_r values were similar. The data indicates that λ_τ dependence on L and τ of the layers with diffusely reflecting surfaces is described with a good approximation by (1) and similar formulas. In contrast, the experiments with a polished aluminum boundary (cold) surface

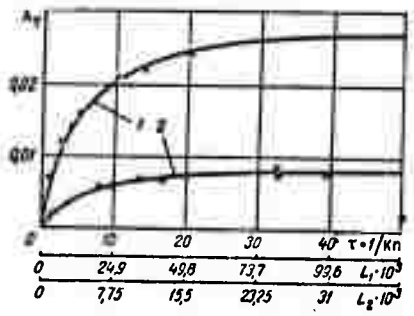

Fig. 1. λ_T in W/m/degree vs. optical thickness τ and L(m m) of a loose fibrous layer of 30 kg/m^3 volume density, $\epsilon_r = 0.27$. Solid lines are calculated by (1)
1- caprone fiber, 2- super-thin glass fiber

revealed a significant discrepancy with the theoretical data calculated by (1). It was concluded that the $\overline{\mu} = 3/2$ value is acceptable only for gray, diffusing boundary surfaces of thin layers of any τ, i.e. the boundary boundary has the effect of increasing τ by a constant value.

Burakov, V. S., P. A. Naumenkov, V. P. Ivanov, and G. A. Kolosovskiy. Study of the passage of powerful laser radiation through an optically dense plasma. ZhPS, v. 16, no. 2, 1972, 239-242.

Some nonlinear absorption characteristics of laser propagation through a plasma are described. The plasma used was optically dense (4--7/ cm) and at ~4ev in a textolite capillary 2.9 mm in diameter. Transmissibility was measured with a passively Q-switched ruby laser generating a 30 ns pulse at 10^6--10^8 w/cm^2. A pronounced bleaching peak was found at about 10^7 w/cm^2. as seen in Fig. 1. The left-most point of the extrapolated

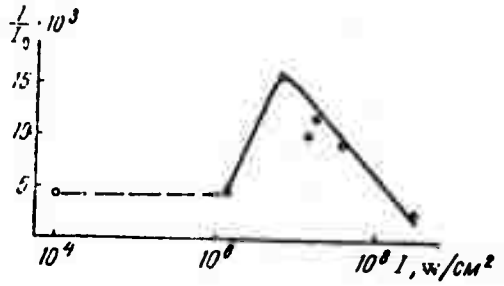

Fig. 1. Plasma transmissibility vs. laser intensity

portion was obtained with a free-running ruby; it was not possible to excite the plasma in the Q-switched mode below 10^6 w/cm^2. The absorption characteristic vs. temperature are given for the HI, CI, OI and CII components. Results indicate the ion and electron temperatures vary almost in synchronism. A general conclusion is that in a multicomponent, highly ionized plasma of the type tested, deviation from equilibrium concentration of electrons can be caused by individual hard-ionizing elements; in the present case this was due to the C II component. It follows that care must be taken to allow for nonlinear absorption when using a powerful laser for certain plasma diagnostics.

Askar'yan, G. A., E. Ya. Gol'ts, and T. G. Rakhmanina. Alteration of the propagation and reflection of ultrasound under the effect of an intense light on the surface of a body in liquid. ZhETF, v. 62, no. 3, 1972, 1072-1074.

A new effect was investigated experimentally in which the propagation of sound is changed due to intense light acting on the medium. A flash of an unfocused and unmodulated neodymium laser beam sharply reduced the reflection and transmission of ultrasound through the surface of a steel plate immersed in water. Strong change is found when the surface temperature T is high enough to form vapor or gas. An expression was derived for determining this temperature. In the experimental arrangement (Fig. 1), a laser beam

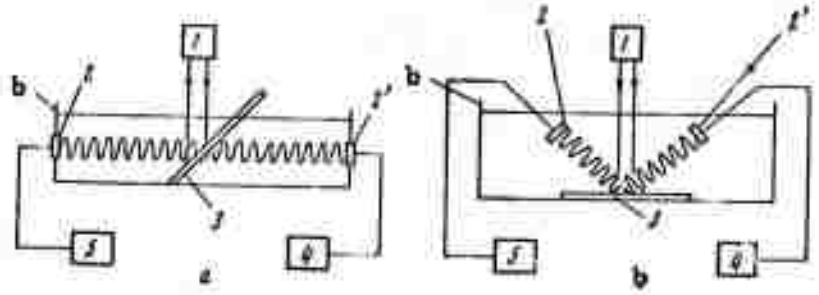

Fig. 1. Experimental sketch for investigating alterations of (a) propagation and (b) reflection of sound due to an unfocused laser beam on the surface.

from 1 falls on the surface of a steel plate 3, immersed in water in vessel 6. An ultrasonic transmitter 2, a piezoelectric element of 1 cm radius, transmits a directional ultrasonic wave at a frequency of 2 MHz from generator 5, in such a way that the sound wave passes through the surface region, illuminated by the laser pulse. The piezoelectric receiver 2' records the ultrasound radiation, passing through (Fig. 1a) or reflected by the plate (Fig. 1b). Two series of experiments were conducted: a) using a free-running laser with a maximum energy ~10 joules, pulse duration ≈0.5 msec, and beam radius 1 cm; and b) using an unfocused, Q-switched laser with a pulse width of 30-40 nsec. Seven oscillographs obtained during the experiments are given to show the effects of light on the reflection of sound. The build-up time of the interaction effect, connected with the formation of vapor-gas bubbles or of a non-uniform film, was commensurate with the energy release time.

Duration of interaction increases with an increase of flux density and at a light flux density of ~10kw/cm^2 lasts for ~200 msec, which significantly exceeds the laser pulse duration (~1 msec). At high laser powers with Q-modulation, a rapid film formation was observed, which eliminated propagation and changed the sound reflection. Possible applications include: the interruption and elimination of reflection and propagation of sound, and ultrarapid modulation of sound, when short laser pulses are used.

Zakharov, V. P., V. N. Chugayev, V. I. Zaliva, and Yu. G. Poltavtsev. Study of the graphitization process of thin carbon films from the effect of powerful light pulses. UFZh, no. 2, 1972, 279-283.

An experiment in optical graphitization of a carbon film is described, which complements the work of Zakharov reported previously (March 1972 monthly report, p. 9 and April report, p. 130). Instead of a laser a type IFP flashlamp was chosen in the present case, having a spectral peak at 0.4 micron, and used to irradiate a 10^{-5} cm pure carbon film at various distances and flash intensities. The bulk of the experiment was devoted to increasing change in optical transmission of the film, giving an index of the induced graphitization process. A typical result is shown in Fig. 1.

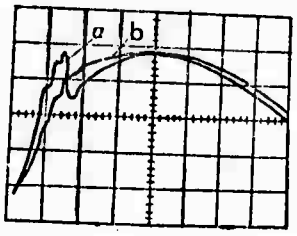

Fig. 1. Change in transmitted flux of irradiated carbon film.
a- after first pulse;
b- after second pulse
major division = 10^{-4}sec.

For this case a film area of 1 cm^2 was determined to be raised to the order of 1000°C per pulse. Curve (a) in the figure shows the inflection interval where graphitization occurs; the reduced response of curve (b) then held true for subsequent pulses. In this case graphitization occurred in about 10^{-5} sec.; correspondingly increased times were required for reduced film treating rates. The authors suggest a two-step process occurring, beginning with a rapid formation of crystallites, and followed by a more extended period of crystallite reorientation and grouping into the graphite structure. Additional tests on r-f transmissibility of the exposed film confirmed the assumed process.

Mirkin, L. I. Dynamic deformation of low-carbon steel from the effect of a laser beam. IN: Sbornik. Vysokoskorostnaya deformatsiya. Moskva, Izd-vo Nauka, 1971, 109-112. (RZhMekh, 9/72, # 3V1469)

Structural effects are studied in low-carbon steel exposed in vacuums to focused laser pulses in the 1 millisecond range, at energies up to 35 j. The amount and distribution of resultant twinning was measured. A physical model of the beam action is postulated to explain the simultaneous presence of a thermal and mechanical interaction zone.

Gurevich, V. I. Pulse forms of a periodic point source of heat on the surface of a large body. FiKhOM, no. 2, 1972, 19-22.

A study on the effect of pulse shape on laser interaction with metals was mentioned by Baranov, Gurevich, and Heinrichs in a previous report (April Monthly Report, p. 4). In the present paper Gurevich gives a more extended analysis of pulse shape effect. The model assumes a periodic pulse from either a stationary or moving source, and is used to calculate a limiting temperature field in the impact region at the conclusion of the laser pulse; for convenience a dimensionless temperature θ_i is introduced. Analytical expressions for θ_i' (fixed) and θ_i'' (moving source) are then obtained in terms of beam parameters and the Fourier (Fo) and Peclet (Pe) criteria. A comparison of pulse shape effect on θ_i' is seen in Fig. 1 for the fixed source case, showing the maximum effect of a sawtooth pulse

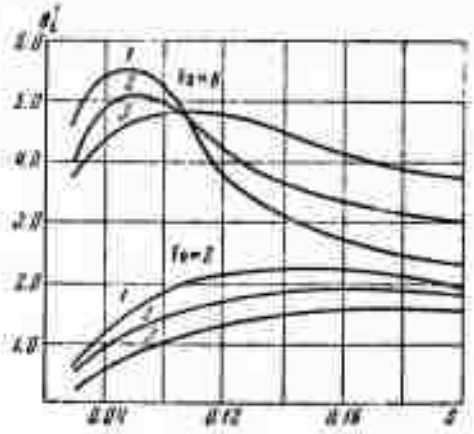

Fig. 1. Temperature θ_i' vs. duty factor S
1- sawtooth pulse, vertical leading edge;
2- rectangular pulse;
3- sawtooth, vertical trailing edge

with vertical leading edge, at the higher Fo levels. It follows that this form would be preferable for fast local heating of a limited surface area, despite the fact that a $\sin^2$ pulse generally gives most efficient energy transfer in a given pulse width. Tabulated results are also included comparing the limit temperatures for a moving beam in terms of the cited pulse shapes, again showing the superiority of the vertical-rise sawtooth.

Kapel'yan, S. N., and A. M. Yudovin. Duration of vaporization after termination of a powerful thermal flux. DAN BSSR, no. 3, 1972, 214-216.

Theoretical expressions are developed which define post-pulse vaporization duration, as well as depth of the vaporization layer, for the case of laser irradiated metals. The work is based on heating concepts reported by Anisimov (Effects of High Power Lasers, Dec. 1971, p. 24) and uses his thermophysical model. This asserts that the thermal field at the conclusion of a rectangular pulse can be given by

$$T(x) = T_0^* \exp(-\beta x) \qquad (1)$$

where $1/\beta = a/v_0$ is a characteristic dimension of the heated region, and T_0^* is the temperature at the vaporization front. Following the laser pulse the vaporization front will continue to expand until T^* drops to vaporization threshold. This interval can be found from a transcendental equation expressing vapor kinematics and target thermal parameters; the authors obtained solutions by simple iteration using a Minsk-22 computer. Results for several metals are seen in Fig. 1, showing that at a given laser flux

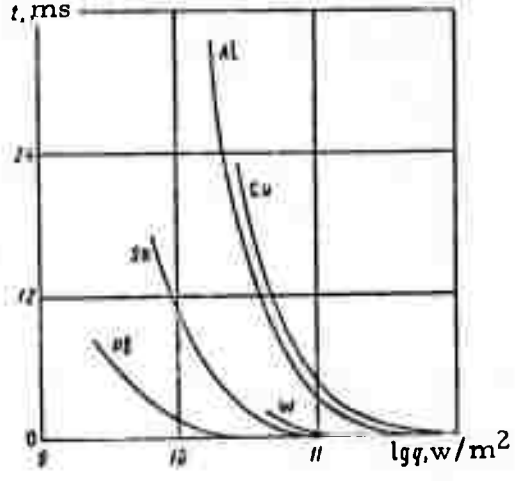

Fig. 1. Post-pulse vaporization duration vs. laser intensity

the longest post-vaporization will occur in Cu and Al, and the shortest in Pb. The sharp decrease in post-pulse vaporization with rise in pulse intensity is shown to be consistent with the thermal storage mechanisms in the impact region.

Pustovalov, V. K. Self-similar gas motion behind a shock wave front sustained by radiation. DAN BSSR, no. 12, 1971, 1079-1081.

The author analyzes a simple model which relates to the optical plasmatron described by Rayzer and others (see for example the February 1972 Monthly Report, p. 11), i. e. a continuous local plasma sustained by a laser beam. The present model assumes a half-space $x > 0$, filled with a cold ideal gas of constant density ρ, where the surface $x = 0$ is the boundary between the gas and vacuum. At time $t = 0$ a strong shock wave begins to propagate from the boundary in to the gas, impelling the gas to expand into the vacuum. Energy from an optical flux q is absorbed by the gas and uniquely determines the propagation of the shock wave; gas expansion is assumed to be adiabatic. Using this model, the author develops self-similar equations in Euler coordinates defining gas pressure, density, velocity in terms of adiabatic index γ and the self-similar index ξ. It is shown that for the sustained shock condition γ must lie between 1 and 1.5. The case of $q < 0$, i. e. energy radiating from the shock wavefront, is also briefly considered.

VIII. PARTICLE BEAMS

Gaponov, V. A., and V. S. Nikolayev. Accelerator tube. Author's certificate USSR no. 299989, published March 26, 1971, 2 p.

An accelerator tube with magnetic focusing lenses is introduced. The tube consists of sectionalized insulated segments and electrodes. With the aim of increasing the electric field gradient along the tube, plates are placed on the electrodes near the aperture for charged particle beam transmission. The plates are located on alternate electrodes in a diametrically opposite manner, forming a periodic inclined system. The plates are comb-shaped with teeth equivalent to elementary Faraday cylinders. Details of the accelerator tube are shown in Fig. 1.

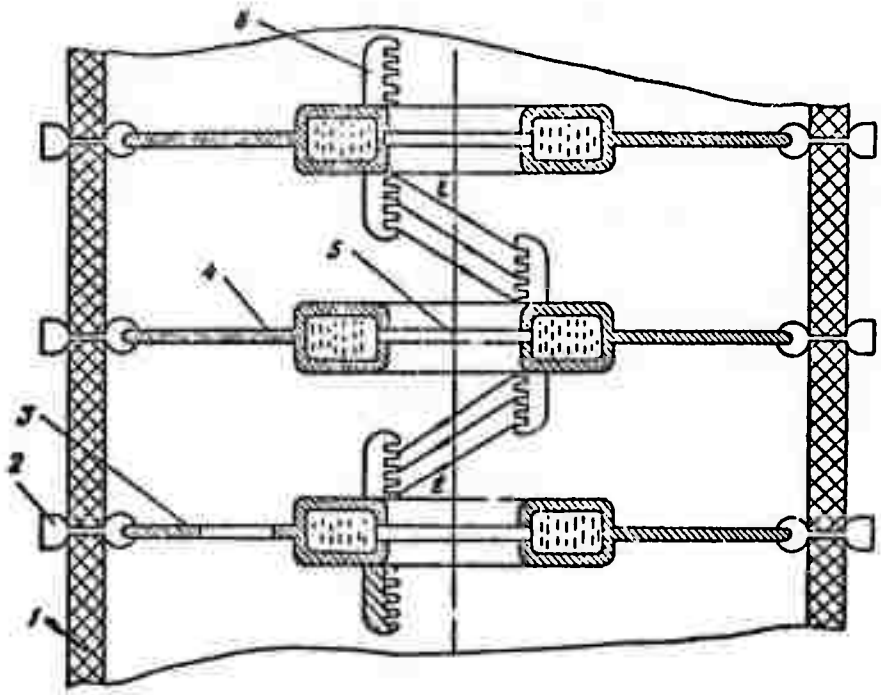

Fig. 1. Section of accelerator tube.
1- accelerator ring
2- split metallic electrodes
3- internal electrodes
4- focusing magnetic lenses
5- apertures
6- flat plates
E- electric field

Kul'man, V. G., E. A. Mirochnik, and V. M. Pirozhenko. Linear charged particle accelerator. Author's certificate USSR no. 279822, published March 26, 1971, 2 p.

A linear charged particle accelerator operating on a $\pi/2$ wave is described. The accelerator consists of H-profile accelerating and coupling elements with coupling windows. To increase the coefficient of cell coupling, the cells are in the form of ring resonators. The connecting windows between the accelerating and coupling cells are placed with a mutual relative offset in azimuth. The design provides for simple welding of sections and ease of evacuation. Details are shown in Fig. 1.

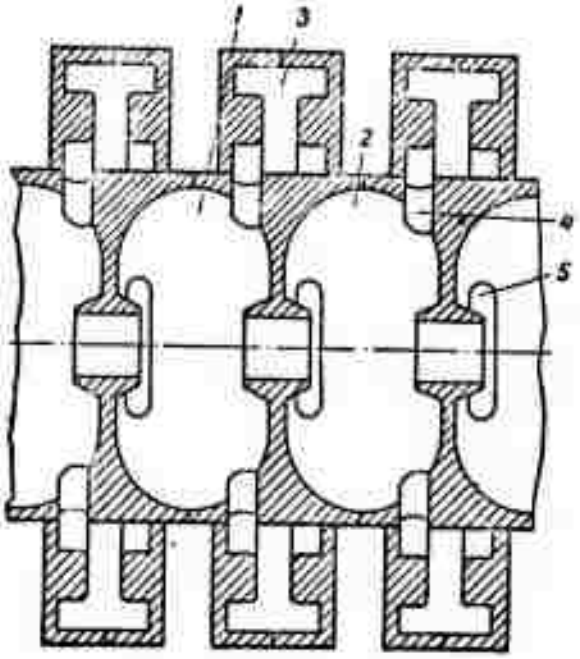

Fig. 1. Section of linear accelerator.
1, 2- Toroidal accelerating cells
3- Coupling cells
4, 5- Coupling windows

Rukhadze, A. A., and V. G. Rukhlin. Injection of a relativistic electron beam into a plasma. ZhETF, v. 61, no. 1, 1971, 177-189.

This article deals with theoretical asymptotic investigations of induced charges, currents, and electromagnetic fields, resulting from the injection of an electron beam into a plasma. The plasma was assumed to be free of other external fields. Only high-speed processes were taken into account; thermal movements of particles were neglected. Mathematical expressions were obtained for induced charges, currents, magnetic fields, and dielectric permeability. The problem is represented by a series of mathematical terms, so that the general formulas obtained can be applied to systems at any moment of time during the injection of a finite length electron beam into the plasma. At conditions $r_0 > c/\omega_p$, where r_0- beam radius and ω_p- plasma frequency, plasma perturbations are localized in the region of the electron beam itself; and currents induced in the plasma tend to compensate the beam magnetic field, facilitating its injection into the plasma. If the beam injection time $\tau > \tau_0 = \gamma^{-1} (r_0 \omega_p/c)^2$ (where γ is the plasma electron collision frequency), magnetic field compensation occurs at distances $z < z_0 = u\tau_0$ from the beam front, where u is the directed electron velocity. For a high-current electron beam when the magnetic energy of beam current exceeds the kinetic energy of electrons, simplified injection into a dense plasma is possible only for the case where $\omega_p > c/r_0$ and $\tau < \tau_0$.

Vagin, Yu. P., G. L. Kabanov, Yu. A. Medvedev, and B. M. Stepanov. Method of visualizing space distribution of dose in a powerful pulsed high-speed electron beam. Atomnaya energiya, v. 32, no. 1, 1972, 73-75.

The scattering field of high-speed electrons, and the luminosity field in air were investigated by photoelectronic and photographic methods; and luminosity field characteristics were compared with results of approximation theory on multidimensional electron scattering. Electron beams of 1 and 4 Mev were used with a pulsed electron current of 0.1 and 3.0 a, a pulse duration of 2 and 1.2 μsec, and a frequency of 400 and 25 Hz, respectively. Electron beams were dispersed in air forming a typical luminous cone. A photoelectronic detector (an FEU and Faraday cylinder) simultaneously recorded the luminous intensity and electron current. Luminescence was observed in a small volume of air (~1 cm^3), placed in the Faraday cylinder and confined by an inlet diaphragm (~1 cm). The results are given of measurements of the luminescence intensity and the electron current in a lateral cross-section of an electron beam at a distance of 3 cm from the outlet window of the accelerator (Fig. 1). Measured by three different methods,

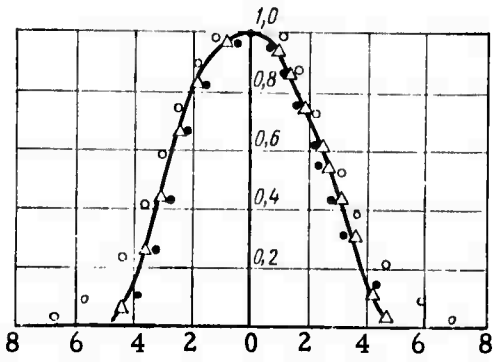

Fig. 1. Lateral distribution of the intensity I of luminous air. (• - photoelectronic method; o- photographic method) and electron current with 1 Mev energy (Δ)

the results are in good agreement and deviate from the mean Gaussian distribution curve by not more than ± 10%. The comparison of experimental results with calculations using approximation theory on multidimensional electron scattering is plotted in Fig. 2. These results agree well for the 4 Mev electron beam; however, for the 1 Mev beam satisfactory agreement began to appear only at a distance of about 10 cm.

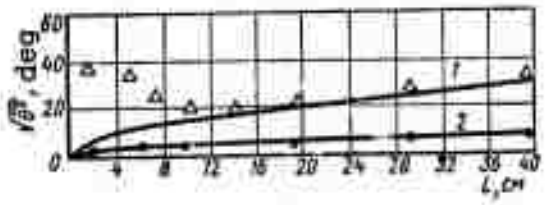

Fig. 2. Relationship of electron scattering angle 0 in air to distance L along the beam axis.
1, 2 - calculated curves for 1 and 4 Mev electrons
•, Δ - experimental curves for 1 and 4 Mev electrons

IX. ELECTROMAGNETIC FIELD INTERACTION WITH MATERIALS

Balkarey, Yu. I. and E. M. Epshteyn.
Coulomb shielding in a strong electromagnetic field. FTT, no. 3, 1972, 741-745.

The effect is analyzed of a strong electromagnetic field on the shielding of a static charge by an electron cloud in the electron plasma of a crystal. A dipole approximation is introduced on the assumption that the e-m wave amplitude varies over a distance greater than the charge dimension, the Debye shielding radius, and the electron oscillatory amplitude. In a collisionless plasma, the condition $\omega_p \tau \geq 1$ must be satisfied, where ω_p is the plasma electron frequency and τ is the electron relaxation lifetime. An integral equation of the scalar potential function $\varphi(q, t)$ was derived in an approximation of chaotic phases from the wave equation using Poisson's equation. The potential φ describes the static charge field. Using the known expansion of the Bessel function $J_s(z)$, the constant component of φ is expressed by

$$\varphi_0(r) = \int \varphi_0(q)\, e^{-iqr}\, \frac{dq}{(2\pi)^3} = \int \frac{dq}{(2\pi)^3}\, e^{iqr}\, \frac{4\pi\rho(q)}{q^2} \sum_{s=-\infty}^{+\infty} \frac{J_s^2(aq)}{\varepsilon(q, s\Omega)} \qquad (1)$$

where r is the distance from the shielded charge to the observation point, q is a coordinate in the Hamiltonian of the analyzed system, $\rho(q)$ is the Fourier component of a static charge, a is the oscillatory amplitude of electrons in the wave field, $\epsilon(q)$ is the static dielectric constant, and Ω is the electromagnetic field frequency. By introducing

$$\frac{1}{\varepsilon_{eff}(q)} = \sum_{s=-\infty}^{+\infty} \frac{J_s^2(aq)}{\varepsilon(q, s\Omega)} \qquad (2)$$

in (1), a formula for the effective static dielectric constant $\epsilon_{eff}(q)$ is obtained. The formula (1) together with (2) describe the effect of an electromagnetic wave on static distribution of φ.

The component $\varphi_0(r)$ of φ is calculated on the assumptions that the shielded charge is a point charge ($\rho(q) = Ze$), $\Omega \geq \omega_p$, and r satisfies inequalities $r \geq \lambda$ and $\chi r \geq 1$, where λ is the characteristic electron wavelength

and χ is the Debye radius reciprocal. Under these assumptions, (1) becomes

$$\varphi_0(r) = \frac{4\pi Ze}{\epsilon_0} \int \frac{dq}{(2\pi)^3} \frac{e^{iqr}}{q^2} \left[1 - \frac{\chi^2}{q^2 + \chi^2} J_0^2(aq)\right] \qquad (3)$$

When a is much smaller than the Debye radius ($\chi a = F \leq 1$), the formula (3) is approximated by

$$\varphi_0(r) = \frac{Ze\chi}{\epsilon_0} \left\{ \frac{e^{-R}}{R} \left[1 + \frac{F^2}{2}\left(\cos^2\alpha + \left(\frac{1}{R} + \frac{1}{R^2}\right)(3\cos^2\alpha - 1)\right)\right] - \right.$$
$$\left. - \frac{F^2}{2R^3}(3\cos^2\alpha - 1) \right\}, \qquad (4)$$

where $R = \chi r$, and α is the angle between the r and E_0 vectors.

In the presence of an electromagnetic field, it follows from (4) that the potential distribution is anisotropic and contains exponentially decreasing terms which predominantly contribute to the φ_0 value at long distances. An electromagnetic wave thus induces a "shielding breakdown". At $R \longrightarrow \infty$, $\varphi_0(r)$ acquires a quadrupole instead of a dipole form, because the average dipole moment is zero in a high-frequency field. If $R \geq \max(2F, 1)$ and $\alpha = 0$, it follows from (4) that φ_0 acquires the asymptotic form $\varphi_0 = -(Ze\chi/\epsilon_0)(F^2/R^3)$, regardless of the F value.

Analogous mathematical operations, using linearized equations of motion and continuity, led to the conclusion that formulas (1) and (2) are also applicable for frequent collisions in an electronic gas, when $\omega_p \tau \leq 1$. Formulas (3) and (4) are also satisfied if the condition $\Omega \geq \omega_c$ (where $\omega_c = D\chi^2$ is the reciprocal of the Maxwellian relaxation lifetime and D is the diffusion coefficient) is substituted for $r \geq \lambda$ and $\chi r \geq 1$. In contrast to the collisionless plasma, the formulas of a and $\epsilon(q, \omega)$ are explicit.

In summary, "breakdown" of shielding occurs at a sufficiently high e-m field frequency regardless of the status of collisions in the electron gas. Numerical calculations show for example that the condition $\Omega \geq \omega_p$ is satisfied for n - InSb with an average electron concentration $N_0 \cong 10^{16}$ cm^{-3} at $\Omega \cong 10^{14}$ sec^{-1}. At low temperatures, $E_0 \cong 10^5$ V/cm is required to achieve $F \cong 1$. The condition $\Omega \geq \omega_c$ is satisfied for n-Si with $\rho \sim 10^3$ ohm x cm at $\Omega \cong 10^{10}$ sec^{-1} and room temperature; $E_0 \cong 10^3$ V/cm is sufficient to achieve $F \cong 1$. The examples demonstrate that the "breakdown" of shielding can occur at reasonably attainable field values in the i-r and shf ranges.

Bozhkov, A. I., and F. V. Bunkin. Optical excitation of surface waves in transparent condensed media. ZhETF, v. 61, no. 6, 1971, 2279-2286.

The excitation of surface waves in condensed media by two mutually interfering plane monochromatic waves is discussed. Optical excitation of surface waves in such a case proceeds by a striction mechanism which involves a ponderomotive force jump from the normal to the surface component. The mechanism is not related to radiation absorption and hence is primarily applicable to transparent media. The proposed method of surface wave excitation is examined for two coherent monochromatic waves incident on a liquid surface. Mathematical treatment of an equation of motion of the liquid-atmosphere interface, with allowance for ponderomotive forces, produced general formulas of the velocity component V_z and the function $\zeta(x, y, t)$ describing surface deviation from the $z = 0$ plane. These formulas led to the conclusion that two plane electromagnetic waves stimulate vibrations of the liquid surface with amplitude $|\zeta_0|$, a wave vector $q = k_{t1} - k_{t2}$, and a beat frequency $\Omega = \omega_1 - \omega_2$. In these expressions, k_{t1} and k_{t2} are the wave vector projections on the liquid surface, and ω_1, ω_2 are the frequencies of the two optical beams. A formula was derived for $|\zeta_0|^2$ as a function of q, Ω, which is applicable also to a total Fresnel reflection, when the liquid occupies a space $z > \zeta(x, y, t)$. Analysis of frequency characteristic $|\Delta|^{-2}$ variations as a function of Ω in the regions of low and high Ω revealed that $|\Delta|^{-2}$ for viscous liquids decreases continuously with increases in Ω, and the $|\Delta|^{-2}$ characteristic for low viscosity liquids is a resonance frequency in the region of high Ω. For $\Omega = 0$, the $|\zeta_0|$ of the static surface wave is independent of viscosity γ and in the cases of $\Omega = \Omega_0(q)$ and $\geq \Omega_0^2 / \nu q^2$ the surface wave travels with $|\zeta_0|$ dependent on ν, surface tension and α, dielectric constant of the liquid, and independent of ν and α, respectively. Conditions are given for the application of the $|\zeta_0|$ formulas to a laser excitation source. Examples of numerical evaluations of the optical beam intensities required to stimulate surface waves in a high or a low viscosity liquid show that striction can stimulate these waves with an amplitude much higher than thermal excitation, and in certain cases may determine the radiation resistance of transparent laser materials.

Myshenkov, V. I. and Yu. P. Rayzer. Ionization wave propagating as a result of resonance quanta diffusion and sustained by shf radiation. ZhETF, v. 61, no. 5, 1971, 1882-1890.

Sustained propagation of an ionization wave in noble gases in an shf electric field E was analyzed. The wave propagates at a power density far below the threshold density of gas breakdown. The simplified scheme of steady-state propagation involves: energy transfer from the shf field to electrons, atom excitation to a single resonance state, and ionization of the excited atoms by electron shock and diffusion of plasma resonance radiation into undisturbed layers. In the one-dimensional model of the reference coordinate system (Fig. 1) the ionization wave is at rest in the system. The

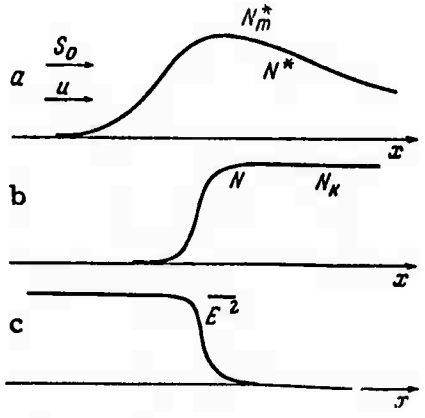

Fig. 1. Schematic parameters distribution in a two-dimensional steady-state ionization wave: a - density N* of excited atoms; b - electron density N; c - mean square shf field $\overline{E}^2$. Arrows indicate directions of propagation velocity u of nonionized gas in the wave and energy flux S_0 of the incident electromagnetic wave.

wave propagation is described by the simplified equations:

$$udN/dx = \alpha NN^*, \quad \alpha = \overline{v\sigma_i^*(v)}, \tag{1}$$

where α is the ionization rate constant, V is the electron velocity, and σ_i^* is the ionization cross-section of an excited atom;

$$u\frac{dN^*}{dx} = D\frac{d^2N^*}{dx^2} + \frac{\sigma\overline{E}^2}{l^*} - \frac{N^*}{T} \tag{2}$$

where D is the diffusion coefficient, T is the average lifetime of the excited state, and I* is the excitation pctential; and

$$\frac{d^2E}{dx^2} + \frac{\omega^2}{c^2}\left(\varepsilon' + i\frac{4\pi\sigma}{\omega}\right)E = 0, \tag{3}$$

where ω is the electric field frequency, and ϵ' is the dielectric constant.

Approximate solution of (1), (2), and (3), with allowance for boundary conditions, gives the unknown functions

$$N(x) = N_0 e^{\gamma(x)}, \quad \gamma = \frac{\alpha}{u}\int_{-\infty}^{x} N^* dx, \tag{4}$$

where

$$\gamma(x) = \frac{\alpha S_1}{uI^*\sqrt{u^2+u^{*2}}} \cdot \begin{cases} \Delta_1 e^{x/\Delta_1}, & x \leqslant 0 \\ \Delta_1 + \Delta_2(1 - e^{-x/\Delta_2}), & x \geqslant 0 \end{cases} \tag{5}$$

$$N^*(x) = \frac{S_1}{I^*\sqrt{u^2+u^{*2}}} \cdot \begin{cases} e^{x/\Delta_1}, & x \leqslant 0 \\ e^{-x/\Delta_2}, & x \geqslant 0 \end{cases}, \tag{6}$$

where

$$\frac{1}{\Delta_{1,2}} = \frac{u}{2D}\left[\sqrt{1+(u^*/u)^2} \pm 1\right], \quad u^* = \sqrt{4D/T}. \tag{7}$$

and

$$\frac{dS}{dx} = -\mu S, \quad \sigma\overline{E^2} = \mu S, \tag{8}$$

where

$$S = S_1 e^{-\tau(x)}, \quad \tau(x) = \int_{-\infty}^{x}(\mu - \mu_0)dx, \tag{9}$$

S and $S_1 = S_0(1 - \rho)$ are the total and dissipative electromagnetic energy fluxes, ρ and μ are the coefficients of reflection and absorption, τ is the relative lifetime of an excited atom, and u* is the characteristic velocity. Using (4), (5), and (7), formula (10) is derived,

$$N_k = \left[\frac{\alpha S_1 \ln(S_1/S_k)}{\beta b u I^*\sqrt{u^2+u^{*2}}}\right]^b, \quad S_1 = S_0[1 - \rho(N_k)] \tag{10}$$

where β and b are constants. The maximum electron density N_k in the plasma is consequently related directly to u. Using (4), (5), and (8) and approximating S(x) by the step function $S = S_1$ at $x < 0$, $S = 0$ at $x > 0$, an equation was also derived which correlates u with S_1. N_k (S_1) can then be calculated from (10) and finally, $u(S_0)$ and $N_k(S_0)$. The wave propagation velocity is given by

$$u = \frac{\alpha T}{2\gamma_c I^*} S_1. \tag{11}$$

where γ_c = const, if $u < u^*$. The formula for maximum density of excited atoms

$$N^*_{max} = S_1 / l^* u^* \qquad (12)$$

is derived from (6).

The formulas (4) - (12) and experimental and theoretical data from the literature were used to calculate u, N_k, N^*_m, S_o, and S_1 for Xe at p = 3 torr, under the experimental conditions described by Bethke and Ruess [Phys. Fluids 12, 1969, 822]. The tabulated data show that the calculated u values increase with an increase in shf power, in agreement with the experiment, but are 4--7 times lower than the experimental u. This discrepancy is possibly connected with the low α value used in calculations. The existence threshold of the ionization wave $S = cE^2/4\pi$ was calculated as 0.4 w/cm^2 for Xe and 1.2 w/cm^2 for Ar, which is in reasonable agreement with the experiment.